JCB Journal of Cell Biology

ARTICLE

The septin cytoskeleton regulates natural killer cell lytic granule release

Prasad V. Phatarpekar, Brittany L. Overlee, Alexander Leehan, Katelynn M. Wilton, Hyoungjun Ham, and Daniel D. Billadeau

Natural killer (NK) cell–mediated killing involves the membrane fusion of preformed lytic granules. While the roles of actin and microtubules are well accepted during this process, the function of septins, another cytoskeletal component that associates with actin and microtubules, has not been investigated. Here we show that genetic depletion or pharmacologic stabilization of the septin cytoskeleton significantly inhibited NK cell cytotoxicity. Although the stabilization of septin filaments impaired conjugate formation, depletion of septin proteins had no impact on conjugate formation, lytic granule convergence, or MTOC polarization to the cytotoxic synapse (CS). Interestingly, septins copurify and accumulate near the polarized lytic granules at the CS, where they regulate lytic granule release. Mechanistically, we find that septin 7 interacts with the SNARE protein syntaxin 11 and facilitates its interaction with syntaxin binding protein 2 to promote lytic granule fusion. Altogether, our data identify a critical role for septins in regulating the release of lytic granule contents during NK cell–mediated killing.

Introduction

Natural killer (NK) cells, cytolytic lymphocytes of the innate immune system, play a critical role in the immune response against malignant and viral-infected cells. NK cells detect target cells through the interactions of activating receptors expressed on the NK cell surface with their corresponding ligands, whose expression is generally increased on the surface of stressed cells. NK cells kill their target cells through directed exocytosis of preformed lytic granules containing cytotoxic proteins such as perforin and granzymes at the interface of NK and target cells (Vivier et al., 2008). Degranulation is a well-regulated multistep process, which is set in motion by the initial contact between the NK cell and a potential target cell, leading to conjugate formation. The signals mediated by the activating receptors induce formation and accumulation of polymerized filamentous actin (F-actin) at the NK cell synapse, which is a prerequisite for the formation of a stable synapse and clustering of activating receptors. For directed secretion of perforin and granzymes, lytic granules move along microtubules to converge at the microtubule organizing center (MTOC) and then polarize with the MTOC to the synapse. Once near the synapse, the granules traverse the clearings created by F-actin remodeling to reach and fuse with the plasma membrane and secrete their lytic content into the synaptic cleft through exocytosis (Orange, 2008). Thus, cytoskeletal proteins such as actin and tubulin are essential to mediate NK cell cytotoxicity.

Septins are GTP-binding proteins, of which there are 13 distinct family members in humans. Based on sequence similarity, septins are divided into four groups; septin 2 (septin 1, 2, 4, and 5), septin 6 (septin 6, 8, 10, 11, and 14), septin 7 (septin 7) and septin 3 (septin 3, 9, and 12; Beise and Trimble, 2011). All septins contain a centrally located GTP-binding domain flanked by a polybasic region that can bind to phospholipids on the plasma membrane. Septins interact through their GTP-binding domain and N- and C-terminal regions. Two copies of each septin from groups 2, 6, 7, and 3 form hetero-hexamers or hetero-octamers, which form the building blocks of the higher-order structures. The oligomeric complexes bind end-to-end to form nonpolar filaments that associate laterally to form bundles and other complex structures such as rings (Mostowy and Cossart, 2012). Septins from the same group can substitute for each other in the hetero-oligomeric complexes; however, being the sole member of the septin 7 group, septin 7 is an indispensable subunit of all septin complexes. Septins can act as scaffolds to recruit proteins and facilitate protein–protein interactions at specific subcellular locations in critical cellular processes such as cell division and distribution of plasma membrane–bound proteins. Septin filaments located in the cell cortex provide rigidity to the cell and thereby influence cell shape and motility (Mostowy and Cossart, 2012).

Septins are also implicated in the function of the immune system. Septins have been shown to be part of phagosomes in

Department of Immunology, College of Medicine, Mayo Clinic, Rochester, MN.

Correspondence to Daniel D. Billadeau: billadeau.daniel@mayo.edu.

mouse macrophages and human neutrophils, and the disruption of septin organization or depletion of individual septins inhibits phagocytosis (Huang et al., 2008). T cell–specific knock-out of septin 9 affects T cell development and leads to a concomitant decrease in the number of peripheral $CD4^+$ and $CD8^+$ T cells in mice (Lassen et al., 2013). Septins are also required for cytokine-driven proliferation of T cells (Mujal et al., 2016). Membrane blebbing, excess leading-edge protrusions, increased uropod length, and defective motility observed in septin-depleted T cells have demonstrated a requirement for septins in modulating actomyosin forces during T cell motility (Gilden et al., 2012; Sellin et al., 2011; Tooley et al., 2009). Being an important component of the cellular cytoskeleton regulating fundamental cellular attributes such as shape and motility, septins are likely to play a critical role in lymphocyte cytotoxicity, given its dependence on cytoskeletal rearrangement. However, a role for septins in the cytolytic function of lymphocytes, particularly NK cells, has not been investigated.

In this study, using genetic depletion and pharmacological impairment of septin dynamics, we investigated the requirement of septin filament formation during NK cell cytolytic activity. Herein, we found that while septin filament stabilization impairs conjugate formation and NK cell killing, depletion of septin proteins does not impact conjugate formation or lytic granule accumulation at the cytotoxic synapse (CS). Instead, we find that septins copurify with lytic granules and interact with key synaptic machinery including syntaxin 11 (STX11), a key molecule required for the fusion of lytic granules with the plasma membrane. Altogether, our data highlight a novel role for septins in the regulation of NK cell cytotoxicity.

Results

Septin proteins interact with DOCK8 in NK cells

Mutations in the gene encoding DOCK8, a guanine nucleotide exchange factor for Cdc42, result in a primary immunodeficiency characterized by defects in cellular processes regulated by the actin and microtubule cytoskeletons in several immune cells including NK cells (Biggs et al., 2017). Our previous proteomics and biochemical studies have identified multiple actin regulatory proteins in complex with DOCK8 including Wiskott-Aldrich Syndrome Protein (WASP), vasodialator-stimulated phosphoprotein (VASP), and Ena/VASP-like (EVL; Ham et al., 2013). Upon further inspection of our proteomics data, we find that septin 2, a component of the septin cytoskeleton, is also a putative DOCK8-interacting protein. Immunoprecipitation (IP) of DOCK8 from primary human NK cells revealed interactions with not only septin 2, but also septin 1 and 7 (Fig. 1 A). This might not be unexpected if DOCK8 is interacting with septin filaments, which would contain multiple septin family members. Signaling does not regulate the interaction of DOCK8 with septin family members, as similar amounts of septin 2 and 7 could be coimmunoprecipitated with DOCK8 following ligation of the NK-activating receptors CD16 or NKG2D+2B4 (Fig. 1, B and C).

Septin filaments do not appreciably accumulate at the NK-target CS

Since septin 7 is required for the formation of stable septin cytoskeletal filaments containing septin 2, 6, and 3 family members, we examined the localization of septin 7, as a surrogate as to where septin filaments form, in NK cell–721.221 target cell conjugates. Interestingly, septin 7 accumulated around the NK cell cortex in both primary human NK cells and NKL cells forming conjugates with the 721.221 target cell line (Fig. 2 A and Fig. S1 A). This staining was specific to septin 7, since siRNA against septin 7 led to a substantial reduction in septin 7 staining (Fig. S1 C). In marked contrast, septin 7 demonstrated limited or punctate staining at the CS (Fig. 2 A and Fig. S1 A). In fact, the fluorescence intensity of septin 7 at the CS was reduced compared with that of F-actin, whereas it showed increased intensity along the cell cortex away from the CS (Fig. 2 A and Fig. S1 B; line intensity profiles). Consistent with this, a maximum intensity projection of a *z*-stack image of primary NK cell in conjugate with the 721.221 target cell showed more accumulation of septin 7 in the cell cortex as compared with the CS (Fig. 2 B and Video 1). Last, we found that septin 7 mean fluorescence intensity decreased over time at the CS formed between NK cells and 721.221 target cells (Fig. 2 C). Taken together, these data show that septin 7 primarily localizes at the cell cortex, but does accumulate in puncta throughout the CS.

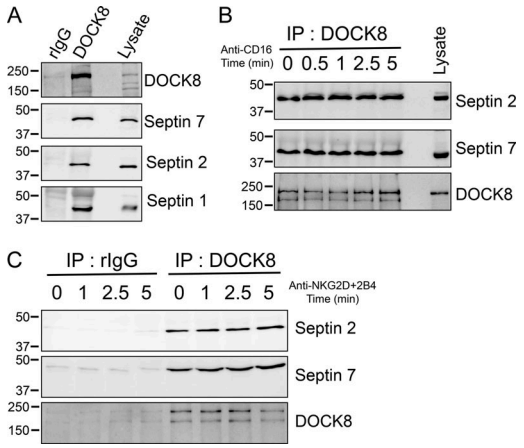

Figure 1. **Septins are DOCK8 interacting proteins. (A)** Primary NK cells were lysed and immunoprecipitated with anti-DOCK8 antibody or rabbit IgG and immunoblotted for the indicated septin proteins and DOCK8. **(B and C)** Primary NK cells were stimulated over the indicated time course by ligation of CD16, the low-affinity FcγRIIIa receptor (B), or NKG2D/2B4 receptors (C), and the indicated proteins were immunoprecipitated and immunoblotted. Representative examples of three independent experiments are shown. rIgG, rabbit IgG.

Septins are required for NK cell–mediated killing

We next sought to determine whether the septin cytoskeleton was required for NK cell cytotoxicity. Initially, we asked whether dynamic reorganization of the septin cytoskeleton is involved in NK cell killing by treating NK cells with forchlorfenuron (FCF), a plant cytokinin that impairs septin dynamics and induces the formation of large septin filament structures (Hu et al., 2008). We found that treatment of either NKL or primary human NK cells with FCF resulted in decreased NK cell cytotoxicity toward Cr^{51}-loaded 721.221 target cells (Fig. S2, A–D). The effect of FCF on cytotoxicity was not due to any effect on cell viability, surface expression of activating

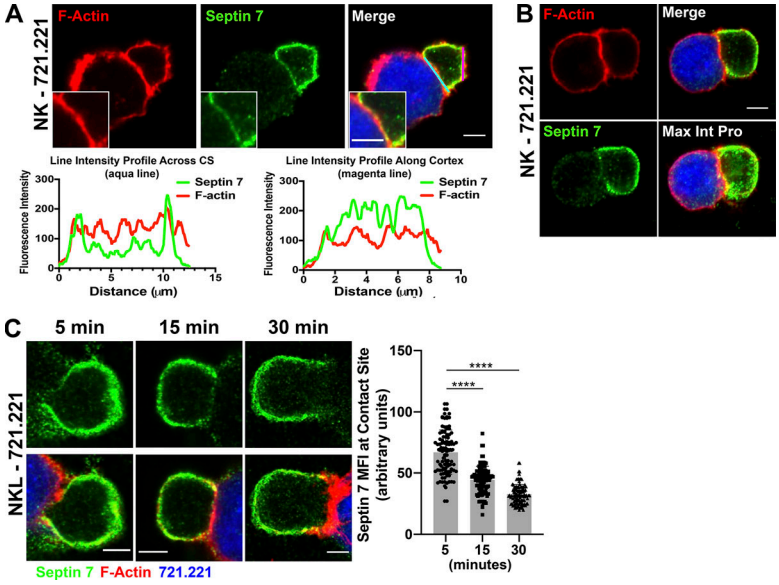

Figure 2. **Septin 7 accumulates around the cell cortex and away from the CS in NK cells. (A)** Primary NK cells were allowed to form conjugates for 15 min with CMAC-labeled 721.221 cells (blue) and stained for F-actin (red) or septin 7 (green) and imaged using confocal microscopy. Scale bar, 5 µm; inset scale bar, 2.5 µm. Line intensities profiles were created from the aqua line at the CS and magenta line along the NK cell cortex in images from A using Fiji. **(B)** NK cell–721.221 conjugates were formed for 15 min, and a z-stack image was obtained for septin 7 (green) and F-actin (red). The individual image shown is slice 6 of 19. **(C)** NK cell–721.221 conjugates were formed at the indicated time points and imaged for septin 7 (green) and F-actin (red). The MFI for septin 7 was measured in 60 conjugates (30 conjugates per time point in two separate experiments) across the CS using ImageJ. The data are graphed and shown to the right of the representative time point images. ****, $P < 0.0001$. P value indicated is for one-way ANOVA with Dunnett's multiple comparison.

receptors, or signals mediated by them, as these parameters were found to be unchanged in FCF-treated NK cells (Fig. S3, A–I). These data indicate that septin filament dynamics are required for NK killing, but whether septin filaments themselves are involved is not known. We therefore depleted septin 7 using siRNA in both NKL and primary human NK cells and examined their ability to kill. Significantly, depletion of septin 7 with two different siRNAs resulted in substantially reduced natural cytotoxicity of both NKL and primary human NK cells toward 721.221 target cells (Fig. 3, A–C and F–H). Moreover, the ability of primary NK cells to kill anti-NKG2D– and anti-2B4–coated p815 cells was significantly reduced (Fig. 3, D and E), indicating that cytotoxicity initiated by these activating receptors requires septin 7, and by extension, septin filaments. Similar results were observed when NKL cells were depleted of septin 2 (Fig. S2, E–I). Altogether, these data indicate that not only do NK cells need to dynamically reorganize their septin filaments to kill, they also require the ability to form septin filaments for the development of their cytolytic function.

It has been previously shown that depletion of septin 7 in mouse T cells (Tooley et al., 2009) leads to the loss of other septin family members, which likely is a result of overall destabilization of the septin cytoskeleton and inability to form normal septin filaments in the absence of septin 7. Consistent with this notion, immunoblotting of lysates from NKL and primary NK cells depleted of septin 7 showed reduced levels of septin 1 and septin 2 (Fig. S4 A). However, when we examined septin 7–depleted NK cells by immunofluorescence (IF), we noted the accumulation of abnormal septin 1 and septin 2 structures consisting of elongated filaments and aggregates within the cell body (Fig. S4 B). These data suggest that the formation of normal septin 1– and septin 2–containing structures in NK cells requires the presence of septin 7.

Stabilization of septins but not loss of septins affects NK cell conjugate formation

Since both septin filament stabilization with FCF and depletion of septin 7 or septin 2 led to defective NK cell–mediated killing, we next sought to determine which stage in the killing process might be impacted. We initially focused on the ability of NK cells to form conjugates, which is among the first steps in the cytolytic process and requires integrin-mediated adhesion and membrane protrusion/remodeling. Consistent with the mechanism of action of FCF, which should impact membrane fluidity by generating a highly stable septin cytoskeleton beneath the plasma membrane, we found that FCF treatment significantly impeded the ability of primary NK cells to spread in response to fibronectin (Fig. S5, A and B) and consequently impaired the ability of NKL cells to form conjugates with 721.221 cells (Fig. S5 C). In contrast, depletion of either septin 7 or septin 2 had no effect on NKL or primary NK cell conjugate formation with 721.221 target cells (Fig. 4, A and B). Taken together, these data indicate that septin filament reorganization, but not septins themselves, are required for conjugate formation.

Loss of septin 7 does not affect lytic granule convergence or MTOC polarization to the CS

Since septin depletion affected NK cell cytotoxicity but did not affect NK cell–target cell conjugation, we next examined whether septin depletion would affect signaling leading to lytic granule convergence to the MTOC or the subsequent polarization of the MTOC and lytic granules to the CS. We therefore deleted septin 7 from NKL cells with CRISPR/Cas9 gene editing (Fig. 4 C), formed conjugates with 7-amino-4-chloromethylcoumarin (CMAC)-labeled 721.221 over time and stained with antibodies for γ-tubulin (to stain the MTOC), perforin (lytic granule), and phalloidin (to stain F-actin at the CS), and measured the distance of lytic granules to the MTOC (convergence) and MTOC to the CS (polarization). As shown in Fig. 4, D–H, deletion of septin 7 had no effect on either lytic granule convergence or MTOC polarization to the CS in conjugates assessed at different time points. Thus, while depletion of septins impair NK cell killing, they do not do so by inhibiting NK conjugate formation or the convergence and mobilization of lytic granules to the CS.

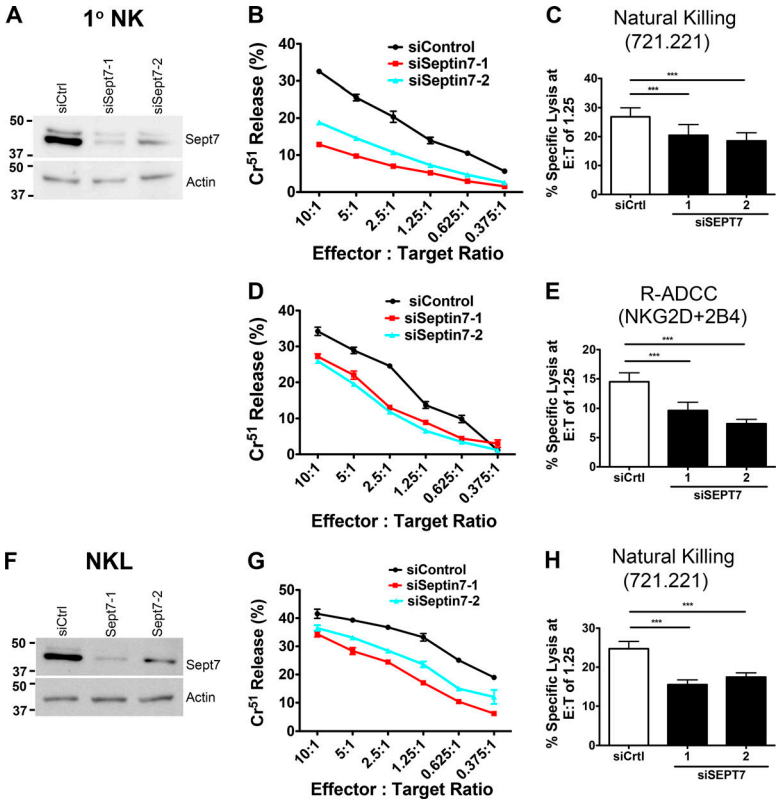

Figure 3. **Septin filament formation is required for NK cell cytotoxicity.** Primary NK (A–E) and NKL (F–H) cells were nucleofected with siCtrl or siRNAs targeting septin 7. Immunoblot is cropped for clarity. **(A and F)** 48 h (primary NK) and 72 h (NKL) after nucleofection, levels of septin 7 protein were assessed by immunoblot for each experiment. **(B and G)** Nucleofected cells were incubated at 37°C for 3 h with ^{51}Cr-labeled 721.221 cells at the indicated Effector:Target (E:T) ratios, and specific lysis was calculated. **(C and H)** Results were quantified for an E:T ratio of 1.25 effectors to one target cell over six independent experiments. **(D)** Primary NK cells were incubated with ^{51}Cr-labeled p815 cells coated with anti-NKG2D + anti-2B4. Percent specific lysis was calculated. **(E)** Results were quantified at an E:T ratio of 1.25 over four independent experiments. All experiments were completed in triplicate or quadruplicate and in reference to spontaneous and total lysis. Results show representative experiments (left and center; A, B, D, F, and G) or average values over multiple experiments (right; C, E, and H). Error bars indicate SEM. ***, P < 0.0005 compared with control group. P values indicated are for paired, two-tailed Student's *t* test. siSept7, siSeptin7.

Septins localize with lytic granules at the CS

Given the fact that septin depletion does not impair the accumulation of lytic granules at the CS, but does affect NK cell killing, we reexamined the localization of septins in NK cells. Although septin 7 staining is reduced at the CS in NK–721.221 conjugates compared with the cell cortex, there remain discrete punctate septin structures throughout the CS contact site as observed by confocal microscopy (Fig. 2, A–C; and Fig. S1, A and B). We therefore reexamined the localization of septin proteins within NK cells and in particular with lytic granules at the CS, since this appeared to be where the defect might lie in septin-depleted NK cells. Using Airyscan imaging, we found that septins 1, 2, and 7 are closely apposed with perforin-containing lytic granules in primary NK cells (Fig. 5 A). In addition, both septin 7 and septin 1 can be found near perforin-containing granules that are localized to the CS formed between a primary human NK cell and 721.221-target cell (Fig. 5 B). The localization of septin 7 with perforin granules at the CS can be further appreciated in the Airyscan-processed *z*-stack orthogonal views, which clearly show the apposition of septin 7 and perforin at the CS (Fig. 5 C). Finally, to determine whether septins might physically associate with lytic granules, we purified the crude lysosomal fraction (CLF) from NKL cells and immunoblotted the presence of co-purifying septin proteins. As expected, the CLF was enriched in granzyme B and LAMP1, major components of lytic granules. Interestingly, and consistent with the imaging data, septins 1, 2, and 7 were also detected in the CLF fraction (Fig. 5 D), suggesting that septin filaments in NK cells can be copurified with the lysosomal fraction.

Septin depletion or stabilization impairs NK cell degranulation

Because septins associate with lytic granules and colocalize with them at the CS, we assessed whether dynamics of the septin cytoskeleton was required for exocytosis of lytic granules. We activated diluent or FCF-treated NK cells using a combination of PMA and ionomycin to artificially stimulate lytic granule release, and measured by flow cytometry (FC) the expression of CD107a (LAMP1), which appears on the NK cell surface upon degranulation. We found that compared with diluent-treated cells, treatment of either NKL or primary human NK cells with FCF resulted in significantly reduced degranulation (Fig. 6, A–F). These data indicate that septin filament dynamics are required for NK cell degranulation. To determine whether septin filaments themselves are involved in degranulation, we depleted septin 7 using siRNA in primary human NK cells (Fig. 6 G) and examined their ability to degranulate upon activation with PMA and ionomycin. Significantly, depletion of septin 7 also resulted in substantially reduced degranulation (Fig. 6, H–J). Taken together, these data indicate that not only do NK cells need to dynamically reorganize their septin filaments to degranulate, they also require the ability to form septin filaments for the degranulation process.

Septins interact with lytic granule fusion machinery

To gain mechanistic insight into septin-mediated regulation of degranulation, we sought to identify the potential protein interactions of septins during the degranulation process. To that end, we activated the human NK cell line KHYG1, a model we previously used to study cytolytic mechanisms in NK cells

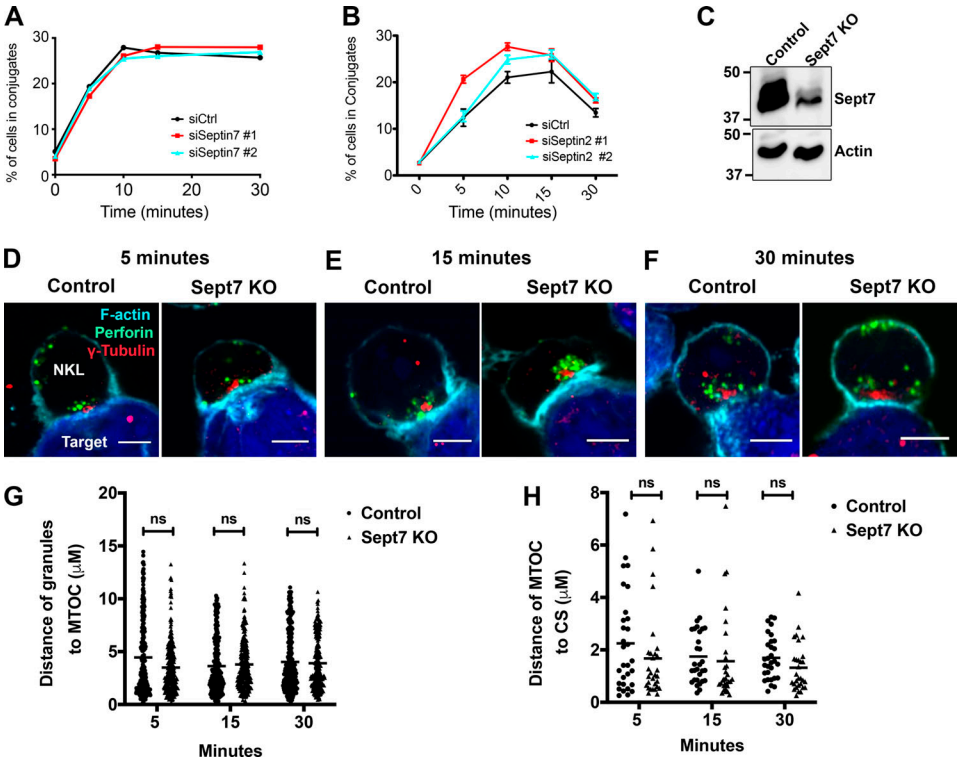

Figure 4. **Depletion of septins does not impact conjugate formation, granule convergence, and MTOC polarization in NK cells.** NKL cells were nucleofected with control or septin 7 or septin 2 siRNAs. **(A and B)** 72 h after nucleofection, NKL cells were stained with Calcein-AM and then allowed to form conjugates at 37°C with CMAC-labeled 721.221 cells over the specified times and then fixed. The formation of conjugates (CMAC + Calcein-AM$^+$) with respect to the total number of NKL cells (Calcein-AM$^+$) was assessed using two-color FC. Results shown are the representative of three independent experiments, each performed in triplicate. **(C)** NKL cells were nucleofected with either control gRNA or two different gRNAs, targeting septin 7 gene (Sept7 KO), in complex with tracrRNA and Cas9 enzyme. 96 h after nucleofection, septin 7 protein expression was assessed by immunoblotting. Immunoblot is representative of three independent experiments. **(D–H)** 96 h after nucleofection, NKL cells nucleofected with control or septin 7 gRNAs were incubated at 37°C with CMAC-labeled 721.221 cells (blue) for the indicated amount of time to allow conjugate formation. Cells were fixed and imaged for the location of the MTOC (γ-tubulin, red) and the location of the lytic granules (perforin, green). The periphery of the cells is defined by F-actin staining (cyan). Granule convergence was measured as the average distance between all of the perforin granules (red) within the NKL cell and the location of the MTOC marked by γ-tubulin. MTOC polarization was measured as the distance between the γ-tubulin location within the NKL cell and the nearest point of synapse with the CMAC stain. **(C–F)** Representative example of NKL conjugates allowed to form for 5, 15, and 30 min. Scale bar, 5 µm. **(G and H)** Granule convergence and MTOC polarization quantified for three independent experiments of 30–50 conjugates per group per experiment. Error bars indicate SEM. ns, not significant. Statistical significance was tested using unpaired, two-tailed Student's *t* test.

(Wilton and Billadeau, 2018; Wilton et al., 2019), with PMA and ionomycin and isolated the CLF. To identify septin-interacting proteins, we immunoprecipitated septin 2 from the CLF and analyzed associated proteins by mass spectrometry. We found a number of proteins with well-established roles in NK cell cytotoxicity. Interestingly, many of these proteins are required for immune synapse proximal terminal steps involved in the cytolytic function of lymphocytes. This finding was in line with our earlier observation that septin filaments and the dynamics of their assembly affect degranulation and cytotoxicity of NK cells without influencing immune synapse distal processes such as granule convergence and MTOC polarization.

The septin-interacting proteins involved in the terminal cytolytic processes included Rab27a, which through its effector protein Munc13-4 helps lytic granules dock and tether to the plasma membrane (Elstak et al., 2011; Feldmann et al., 2003); SNAP23 and VTI1b, SNARE proteins that are part of the trans-SNARE complex formed between lytic granule and plasma membrane during membrane fusion (Dressel et al., 2010; Hellewell et al., 2014; Spessott et al., 2017); and syntaxin binding protein 2 (STXBP2), which promotes trans-SNARE complex assembly (Spessott et al., 2017). SNAP23, VTI1B, and STXBP2 interact with STX11, the target SNARE (t-SNARE) on the plasma membrane essential for membrane fusion and degranulation in the NK cell (Arneson et al., 2007; Bryceson et al., 2007). Interestingly, both STX11 and STXBP2 are also found in the CLF purified from NKL cells (Fig. 5 D).

We next sought to determine whether septins interact with STX11 by immunoprecipitating NKL cell lysate with STX11 antibody. Immunoblotting with septin 7 antibody showed coimmunoprecipitation of septin 7 with STX11 at the basal level as well as upon activation of cell surface receptors (NKG2D + 2B4) or stimulation with PMA and ionomycin, thereby confirming their interaction (Fig. 7 A). The interaction of septin 7 with STX11 did not show any appreciable change upon activation. Moreover, using Airyscan imaging, we could show that septin 7 and STX11 accumulate at the CS formed between NKL and 721.221 target cells (Fig. 7 B). Interestingly, septin 7 shows an

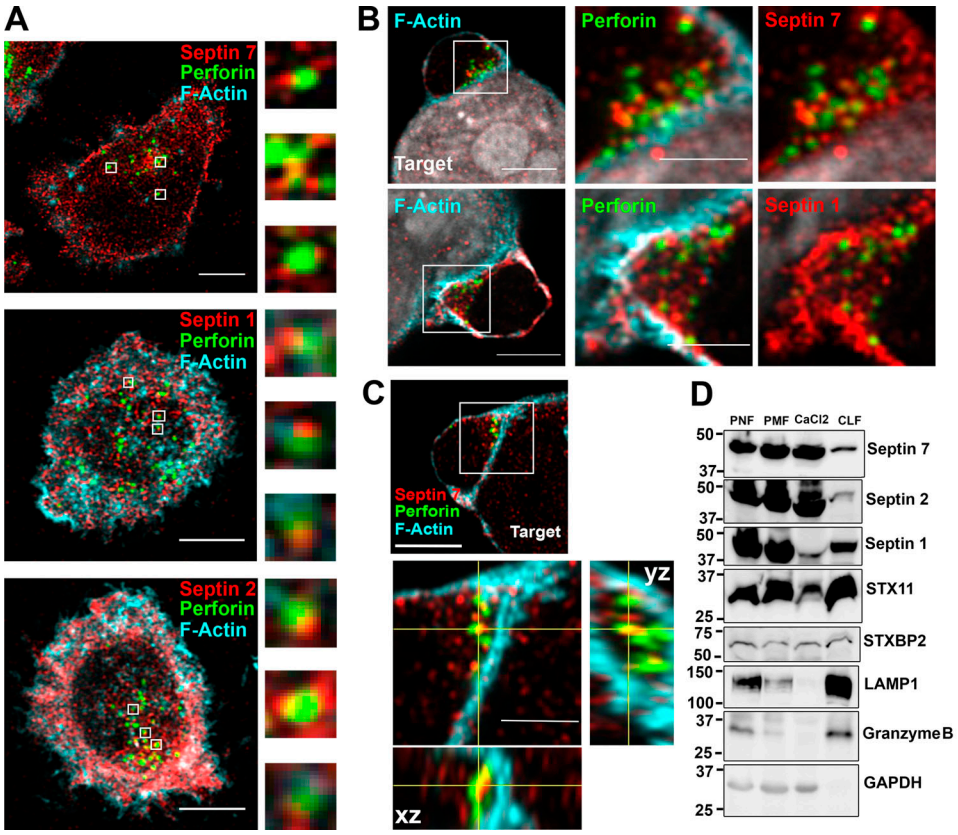

Figure 5. **Septins localize with lytic granules at the CS.** Primary NK cells or their conjugates with 721.221 cells were stained for F-actin (cyan), septin 7, 1, or 2 (red), and perforin (green) to mark lytic granules. Cells were imaged using a confocal microscope in the Airyscan setting. **(A)** Septins were found closely apposed with perforin-containing lytic granules. Representative z-stack images are shown for septin 7 (top; slice 5 of 11), septin 1 (middle; slice 3 of 12), and septin 2 (slice 6 of 12). Scale bar, 5 µm. Magnified images are ∼1 µm. **(B)** Accumulation of septin 7 and septin 1 near lytic granules at the CS. Representative z-stack images are shown for septin 7 (top; slice 19 of 39) and septin 1 (bottom; slice 12 of 20). Scale bar, 5 µm; inset scale bar, 2.5 µm. **(C)** Co-localization of septin 7 with lytic granules at the CS shown in the Airyscan z-stack orthogonal views (slice 14 of 44). Scale bar, 5 µm; inset scale bar, 2.5 µm. **(D)** Postnuclear (PNL), postmitochondrial (PML), $CaCl_2$, and CLF were isolated from unstimulated NKL cells as described in the Materials and methods section and immunoblotted as indicated. Immunoblot is representative of three independent experiments.

almost alternating "beads on a string" pattern with STX11 at the contact site that can be more easily appreciated in the 3D surface plot (Fig. 7 C). Last, using the proximity ligation assay (PLA), a highly sensitive technique to detect protein–protein interactions in situ, we found that septin 7 and STX11 interactions are primarily at the plasma membrane and can also be seen along the CS (Fig. 7 D and Video 2). PLA positive spots could also be observed in the 721.221 target cell lines, suggesting that the septin 7–STX11 interaction is not unique to NK cells. These data suggest that septin 7 makes direct contact with the lytic granule fusion machinery component STX11 at the plasma membrane.

Septin stabilization or depletion impairs interaction between STX11 and STXBP2

STXBP2 is a chaperone protein of STX11 and promotes the trans-SNARE complex assembly between STX11 and other SNAREs and subsequent membrane fusion in human lymphocytes (Spessott et al., 2015, 2017). We assessed whether septins regulate the interaction between STX11 and STXBP2 by analyzing coimmunoprecipitation of STXBP2 with STX11 in NKL cells treated with FCF. Immunoblotting showed decreased STXBP2 expression in STX11 immunoprecipitate from NKL cells treated with FCF. The decrease was observed in nonactivated cells as well as in cell surface receptor (NKG2D + 2B4)–stimulated and PMA- and ionomycin-activated cells (Fig. 8 A), indicating that dynamic reorganization of septin filaments regulates interaction between STX11 and STXBP2. We verified the effect of FCF on the interaction between STX11 and STXBP2 in situ using PLA, which also showed a significantly reduced number of PLA-positive spots in nonactivated as well as PMA- and ionomycin-activated NKL cells treated with FCF (Fig. 8, B and C). Similarly, knock-out of septin 7 in NKL cells led to a significantly reduced number of PLA-positive spots in nonactivated as well as PMA- and ionomycin-activated cells compared with knock-out control cells (Fig. 8, D and E). These data show that formation of septin filaments and dynamics of their organization regulate interaction between STX11 and its chaperone protein, STXBP2.

Discussion

In this study, we show that modulation of septin cytoskeletal assembly either through depletion of individual septins or

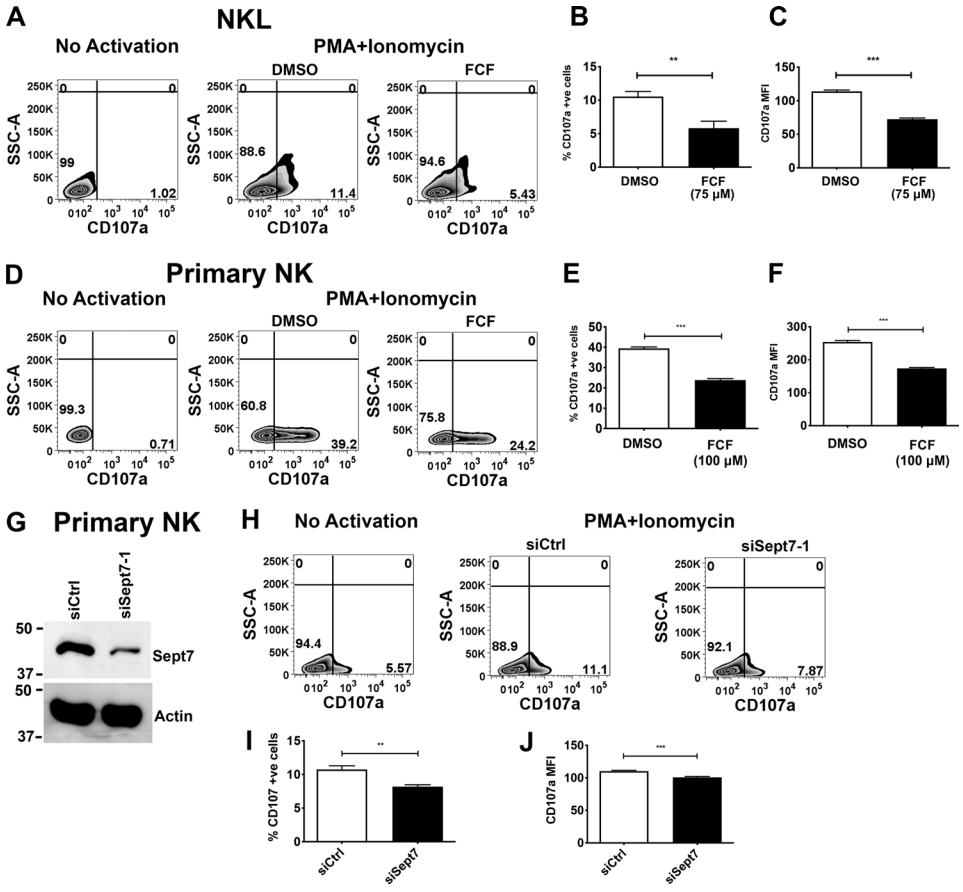

Figure 6. **Stabilization of septin filaments or septin depletion impairs NK cell degranulation. (A–C)** NKL cells were treated with 75 µM and (D–F) primary NK cells with 100 µM FCF for 3 h. **(A and D)** FCF-treated cells were activated with PMA (2 µM) and ionomycin (4 µM) for 30 min at 37°C in the presence of anti-CD107a antibody. Surface expression of CD107a was measured using FC. **(B, C, E, and F)** Percentage of CD107a and MFI of CD107a expression were quantified. **(G)** Primary NK cells were nucleofected with control or septin 7 siRNA. 48 h after nucleofection, levels of septin 7 protein were assessed by immunoblot. **(H–J)** Nucleofected cells were activated with PMA (2 µM) and ionomycin (4 µM) for 30 min at 37°C in the presence of anti-CD107a antibody. Surface expression of CD107a was measured using FC, and percentages of CD107a and MFI of CD107a expression were quantified. Results shown are the representative of three independent experiments, each performed in triplicate. Error bars indicate SEM. **, P < 0.005; ***, P < 0.0005 compared with control group. P values indicated are for paired, two-tailed Student's *t* test. SSC-A, side scatter area.

through pharmacological impairment of dynamics of septin assembly results in inhibition of NK cell cytotoxicity. Our assessment of cellular processes involved in NK cytotoxicity shows that depletion of individual septins does not affect conjugate formation, convergence of granules to MTOC, and MTOC polarization to the synapse, but diminishes degranulation, which we also observe in NK cells treated with FCF, a pharmacological inhibitor of septin assembly dynamics, or depletion of septin 7 (Fig. 9, see legend for details). Mechanistically, we find that septins are associated with lytic granules, and filament stabilization or depletion abrogates the interaction between the SNARE protein STX11 and its chaperone STXBP2, which is required for lytic granule–membrane fusion. Taken together, our results identify a novel and critical role for septins in regulating the release of lytic granule contents during NK cell–mediated killing.

A key step in NK cell–mediated killing is the formation of the CS, which is initiated through integrin-mediated adhesion and plasma membrane restructuring, mainly F-actin–driven protrusions (Pettmann et al., 2018; Segovis et al., 2009). Septin filaments accumulate at the sites of plasma membrane instability and modulate membrane reshaping, particularly protrusions and blebs (Beber et al., 2019; Gilden et al., 2012). Thus, it was not surprising that stabilization of septin filaments with FCF would affect conjugate formation and fibronectin-induced cell spreading. However, given this functional feature of septins, no effect of septin depletion on conjugate formation was an unexpected result. Interestingly, in motile T cells, protrusions formed at the leading edge are sparsely populated by septins, while upon retraction the previously protruded area was found to be enriched with septins (Gilden et al., 2012). This is similar to our observations that the synaptic area was also sparsely populated with septins, but the cortex was enriched in septin filaments. Septins form filaments mostly in the cell cortex and maintain contact with the plasma membrane through direct contact with phospholipids as well as through their association with the actomyosin network in the cortex (Gilden and Krummel, 2010). Thus, a clearing of septin filaments at the contact site would allow more membrane flexibility required for conjugate formation.

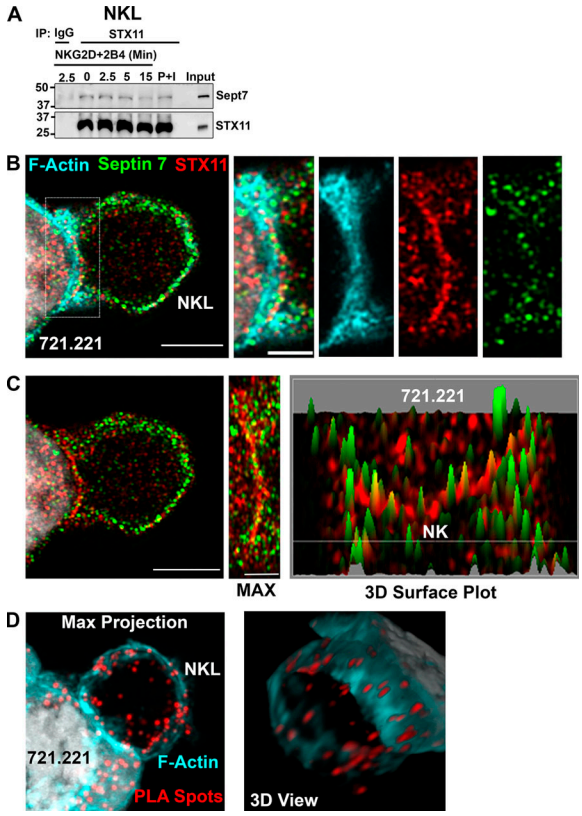

Figure 7. **Septin 7 interacts with STX11. (A)** Unstimulated, cell surface receptor (NKG2D + 2B4) activated (time-course) and PMA (2 µM) and ionomycin (4 µM) (P+I) stimulated (15 min) NKL cells were lysed and immunoprecipitated (IP) with antibody against STX11 or rabbit IgG and immunoblotted as indicated. The immunoblot shown is a representative of three independent experiments. **(B)** NKL cells in conjugates with 721.221 cells were stained for F-actin (cyan), septin 7 (green), and STX11 (red) and z-stack images were obtained and processed using Airyscan (slice 3 of 14 is shown). The localization of the indicated proteins at the CS are enlarged (dashed box) and shown to the right. Scale bar, 5 µm; inset scale bar, 2.5 µm. **(C)** A maximum intensity projection of the Airyscan image for septin 7 and STX11 (from B) is shown with the CS enlarged (middle panel) along with a 3D surface plot (far right) of septin 7 (green) and STX11 (red). Scale bar, 5 µm; inset scale bar, 2.5 µm. **(D)** STX11-septin 7 interaction was also assessed by PLA. NKL cells were incubated with rabbit anti-STX11 and mouse anti-septin 7 antibodies. Subsequently, cells were incubated with plus and minus probes and later ligated and amplified. Cells were stained with phalloidin to visualize F-actin (cyan). Z-stack images were obtained and processed using Airyscan. Representative maximum intensity projection of z-stack and 3D view of the same are shown. Scale bar, 5 µm.

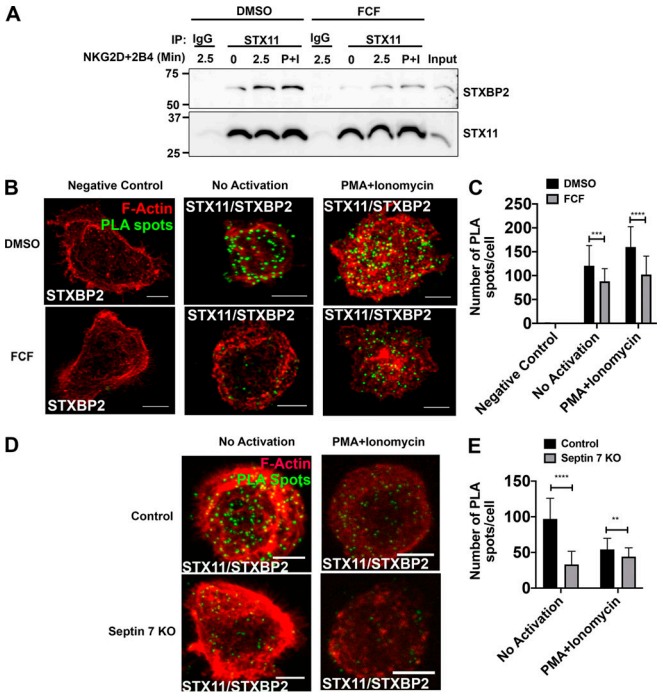

Figure 8. **Stabilization of septin filaments or depletion impairs interaction between STX11 and STXBP2.** NKL cells were treated with DMSO (control) or 75 µM FCF for 3 h. **(A)** Equal number of DMSO- and FCF-treated cells were either not activated or activated by ligation of NKG2D and 2B4 receptors for 2.5 min or PMA (2 µM) and ionomycin (4 µM; P+I) for 15 min at 37°C. Cells were lysed and immunoprecipitated (IP) with anti-STX11 antibody or rabbit IgG and immunoblotted for STXBP2 and STX11. **(B and C)** STX11–STXBP2 interaction was also assessed by PLA. DMSO- and FCF-treated NKL cells were plated on the fibronectin-coated coverslips and incubated with rabbit anti-STX11 and mouse anti-STXBP2 antibodies. Mouse anti-STXBP2 antibody by itself was used as a negative control. Subsequently, cells were incubated with plus and minus probes and later ligated and amplified. Cells were stained with phalloidin to visualize F-actin (red). Z-stack images were captured using a confocal microscope, and PLA spots (green) were counted using ImageJ. Details are described within the Materials and methods section. **(B)** Representative maximum intensity projection of z-stack. Scale bar, 5 µm. **(C)** Quantification of PLA spots. Results shown are representative of three independent experiments with minimum 30 cells counted per group per experiment. **(D and E)** NKL cells were nucleofected with either control gRNA or two different gRNAs, targeting septin 7 gene (Sept7 KO), in complex with tracrRNA and Cas9 enzyme. 96 h after nucleofection, STX11–STXBP2 interaction was assessed by PLA as described above. **(D)** Representative maximum intensity projection of z-stack. Scale bar, 5 µm. **(E)** Quantification of PLA spots. Error bars indicate SEM. **, $P < 0.005$; ***, $P < 0.0005$; ****, $P < 0.00005$ compared with control group. P values indicated are for unpaired, two-tailed Student's *t* test.

Our interest in the role of septins in NK cell cytotoxicity emanated from our finding that septins interact with DOCK8, which we have shown previously to be critical for NK cell cytotoxicity (Ham et al., 2013). Recently, DOCK7 was shown to interact with septins (O'Loughlin et al., 2018), and septin 7 was shown to interact with DOCK8 in equine T cells (Degroote et al., 2014; Schauer et al., 2018). It is well appreciated that septins regulate cell shape and cortical rigidity (Bridges and Gladfelter, 2015), and in murine T cells, this functional attribute of septins is underlined by a cortical array of septins decorating the cell surface (Tooley et al., 2009). Consistent with this established spatial location of septins, we also found that septin filaments mainly accumulated around the NK cell cortex, except in the cortical area of the CS, where weak punctate staining was observed. While the mechanism for septin depletion in this area is not clear, it is of interest that DOCK8 is a guanine nucleotide exchange factor for Cdc42, and a family of effectors of active Cdc42 known as the binder of Rho GTPases (BORGs) are involved in septin filament stabilization until sequestered by active Cdc42 (Farrugia and Calvo, 2017; Joberty et al., 2001; Sheffield et al., 2003). It remains possible that the accumulation of active Cdc42 at the CS by DOCK8 could lead to local septin filament destabilization through the inhibition of BORG–septin

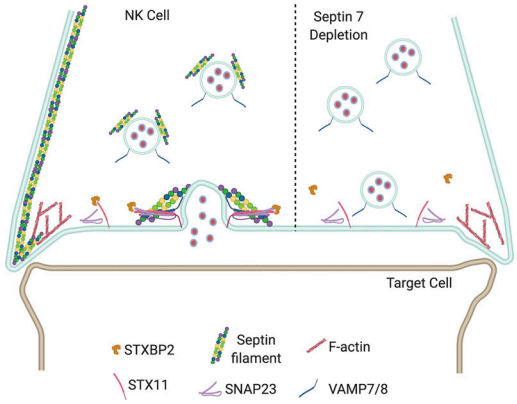

Figure 9. **Model depicting the role of septin filaments in lytic granule release.** Based on the data shown here, we propose that while the septin cytoskeleton is depleted from the CS, it is maintained at the edges of the synapse but is also associated with lytic granules. As a result, septin filaments are brought back to the CS along with the lytic granules, where they participate in stabilizing the STX11:STBP2 interaction to promote lytic granule fusion and release of cytotoxic components. In the absence of septin 7, there is defective lytic granule release due in part to the impaired interaction of STX11 with STXBP2.

filament interactions, which might lead to more membrane dynamics driven by F-actin.

Septin complexes and filaments interact with actin and microtubules, and their spatial and temporal organization are interdependent (Spiliotis, 2018). Even though we did not quantify actin deposition at the CS, its normalcy in septin-depleted NK cells can be inferred from normal conjugate formation, which is an F-actin–driven process. Moreover, depletion of septins did not impact lytic granule convergence to MTOC or the subsequent polarization to the synapse. Since both granule convergence and MTOC polarization are microtubule-dependent processes (Mentlik et al., 2010; Orange et al., 2003), the microtubule network appears to be normal in septin-depleted NK cells. These data are consistent with observations in motile murine T cells, where depletion of septin 7 had no effect on the organization and function of actin and microtubule networks (Tooley et al., 2009). However, it is clear that stabilization of the septin cytoskeleton with FCF does affect F-actin–driven processes such as cell spreading and conjugate formation.

Our data show that septins copurify with lytic granules as well as several proteins involved in the lytic granule degranulation process. In fact, septin 7 coimmunoprecipitates with STX11 and accumulates with STX11 at the CS as determined by both high-resolution Airyscan imaging and the PLA assay. Previous studies in other cell types have implicated septins in the process of exocytosis. Indeed, septins have been found to colocalize with synaptic vesicles in mouse neurons (Beites et al., 1999; Kinoshita et al., 2000; Peng et al., 2002). The interaction of septin complexes with the exocyst complex, which targets and docks secretory vesicles to the plasma membrane, has been shown by coimmunoprecipitation and IF microscopy in rat brain extract and rat neurons, respectively (Hsu et al., 1998), and this interaction has been shown to facilitate secretion from pancreatic-β cells (Rittmeyer et al., 2008). Our data suggest that septin filaments colocalize to the CS through an interaction with lytic granules. It is known that post-translational modification of septins by phosphorylation and sumoylation can alter their activity (Ribet et al., 2017; Yadav et al., 2017). It will be interesting to examine in the future whether the lytic granule–associated septin proteins are regulated by these post-translational modifications and whether such changes influence their ability to promote vesicle fusion at the CS.

Membrane fusion between secretory vesicles and plasma membrane is mediated through trans-protein complex assembly between SNARE proteins located on vesicles and those located on the plasma membrane (t-SNAREs; Tang, 2015). Septins also regulate trans-SNARE formation between vesicle SNARE and t-SNARE on the plasma membrane. In neurons, septin 2 and septin 5 have been shown to directly interact with syntaxin-1, the t-SNARE involved in neurotransmitter release, and septin 5 binds to the trans-SNARE complex formed by VAMP2, syntaxin-1, and SNAP-25 (Beites et al., 1999, 2005). Significantly, alteration of septin filament assembly with FCF disrupts the equilibrium between assembly and disassembly of the SNARE complex and diminishes exocytosis of synaptic vesicles (Nurullin et al., 2019; Tokhtaeva et al., 2015). Interestingly, we also detected PLA positive spots along the plasma membrane not near the CS. This might imply that the exocytosis of other vesicles is also regulated by the interaction of septin filaments with STX11 in NK cells.

We also found septin 2 interactions with proteins involved in membrane targeting, docking, and fusion in NK cells. Septin 2 was found to interact with SNAP-23 and VTI1B, which along with STX11 form the trans-SNARE complex in cytotoxic lymphocytes (Dressel et al., 2010; Hellewell et al., 2014; Spessott et al., 2017), essential for membrane fusion and degranulation in NK cells (Arneson et al., 2007; Bryceson et al., 2007). Since septins are known to bind syntaxin-1 in neurons, we ascertained interaction between septin 7 and STX11 in NK cells. STX11 binds to its chaperone protein STXBP2, which promotes the trans-SNARE complex assembly between STX11 and other SNAREs and subsequent membrane fusion in cytotoxic lymphocytes (Spessott et al., 2015, 2017). We found that deletion of individual septins as well as FCF treatment reduced the interaction between STX11 and STXBP2. Since STXBP2 mediates trans-SNARE complex assembly, the reduced interaction between STXBP-2 and STX11 is likely to diminish trans-SNARE complex formation, resulting in impaired degranulation. Even though the exact role of septins in the binding between STX11 and STXBP2 is not known, based on the colocalization of septin 7 with STX11 at the CS and the well-established role of septin complexes as scaffolds that facilitate protein–protein interactions at specific subcellular locations (Mostowy and Cossart, 2012), it can be argued that septins play a similar scaffolding role in NK cells to mediate and strengthen the interaction between STX11 and STXBP2. Similar to our finding, alteration of septin dynamics by FCF was found to decrease binding of SNAP25, a t-SNARE, with its chaperone, Hsc70, in neuroendocrine PC12 cells (Tokhtaeva et al., 2015).

In conclusion, the data presented here demonstrate a previously unappreciated role of the septin cytoskeleton in NK cell cytolytic function, which is mediated through the regulation of exocytosis of lytic granules. The mechanism proposed here may

not be the only one through which septins regulate exocytosis in NK cells. Studies are underway to understand whether septins also influence processes such as docking and tethering of lytic granules.

Materials and methods

Cells and reagents

All cells were maintained in standard Roswell Park Memorial Institute (RPMI) 1640 with 10% FBS (Sigma-Aldrich or Atlanta Biologicals), and 1% each of penicillin–streptomycin, sodium pyruvate, MEM nonessential amino acids, and glutamine (all from Corning). Primary NK and NKL cell media were supplemented with 50 U/ml recombinant human IL-2 (PeproTech). NKL cells were obtained from M. Robertson (Indiana University Cancer Center, Indianapolis, IN), KHYG-1 cells were obtained from Leibniz Institute DSMZ (Braunschweig, Germany), and 721.221 cells were obtained from the American Type Culture Collection. Primary human NK cells were extracted from anonymized normal donor buffy coats, obtained from the Mayo Clinic Blood Bank (Rochester, MN), using Ficoll-Hypaque (GE Healthcare) and the Rosette Separation NK cell isolation kit (StemCell Technologies, Inc.), as previously described (Wilton and Billadeau, 2018; Wilton et al., 2019). In brief, peripheral blood mononuclear cells were isolated through layering on Ficoll-Hypaque and centrifugation. Total peripheral blood mononuclear cells were then mixed with RBCs at a ratio of 1:100, and Rosette Separation Ab mixture was added and incubated for 20 min at room temperature. Ficoll-Hypaque–mediated separation was repeated, and the resulting NK cells were analyzed for purity by FC using phycoerythrin- and allophycocyanin-conjugated Abs against CD3 and CD56 (BD Biosciences). Cell viability was assessed using Vi-Cell XR cell viability analyzer (Beckman Coulter). PMA was from Sigma-Aldrich, and ionomycin was from MP Biomedicals. FCF 32974 was from Sigma-Aldrich.

Antibodies

Rabbit polyclonal antisera to septin 2 and septin 7 were obtained by immunizing rabbits with GST-conjugated septin 2 aa 279–361 (GenBank, NM_001008491.2) and septin 7 aa 319–417 (GenBank, NM_001788.5; Cocalico Biologicals), which were generated by cloning cDNA sequences into the pGEX-KG GST-fusion vector as HindIII/NotI fragments. cDNA sequences were amplified using forward (5′-CTGAAGCTGAAGCTTATGCTCATCACCCACATG CAG-3′) and reverse (5′-CGACGAGCCGCGGCCGCTTACACGTGG TGCCCGAGAGC-3′) primers for septin 2 and forward (5′-AAG CTTATGGAAGAAGAAAGAAGGGAGCAT-3′) and reverse (5′-GCGGCCGCTTAAAAGATCTTCCCTTTCTTCTTGTT-3′) primers for septin 7. GST–septin fusion proteins were purified and used to generate antibodies in rabbits (Cocalico Biologicals Inc.). The HindIII/NotI fragments were subsequently subcloned into the pMAL expression vector in order to produce maltose-binding protein–septin antigens for coupling to Amino Link (Thermo Fisher Scientific) and antibody purification. Rabbit anti-septin 2 was used for immunoblotting (IB; 1:10,000), and rabbit anti-septin 7 was for IB (1:5,000) and IP. Rabbit polyclonal antisera to DOCK8 and Vav1 (Cocalico Biologicals) were previously generated in our laboratory (Billadeau et al., 1998; Ham et al., 2013). Rabbit anti-DOCK8 was used for IB (1:3,000) and IP, and rabbit anti-Vav1 was used for IB (1:500) and IP. Rabbit antibodies against septin 1 (11370-1-AP) IB (1:500) and IF (1:250), septin 2 (11397–1-AP) IF (1:250), STX11 (13301-1-AP) IB (1:1,000), IP, IF (1:250), and PLA (1:500), and STXBP2 (15312-1-AP) IB (1:1,000) and mouse antibodies against septin 7 (13818-1-AP) IF (1:500) and PLA (1:250), and STXBP2 (66238-1-IG) PLA (1:100) were obtained from Proteintech Group. Rabbit antibodies against CD107a/LAMP1 (9091) IB (1:1,000), ERK1/2 (9102) IB (1:1,000), and phospho-ERK1/2 (4370) IB (1:1,000) were procured from Cell Signaling Technology. Mouse antibodies against phosphotyrosine (05-321) IB (1:1,000), α-tubulin (T9026) IB (1:5,000), and β-actin (A2228) IB (1:5,000), and rabbit antibody against γ-tubulin (T3559) IF (1:250) were obtained from Sigma-Aldrich. Mouse antibody against granzyme B (SC8022) IB (1:3,000) was obtained from Santa Cruz Biotechnology, while mouse antibodies against NKG2D (MAB139) NK cell activation (1:20), and GAPDH (GTX627408-01) IB (1:5,000) were obtained from R&D Systems and GeneTex, respectively. Mouse antibody against perforin (556434) IF (1:1,000), FITC-conjugated mouse antibody against CD107a/LAMP1 (555800) FC (1:5), phycoerythrin-conjugated mouse antibodies against DNAM1 (559789) FC (1:10), LFA-1 (550851) FC (1:10), and CD3 (347347) FC (1:10), and allophycocyanin-conjugated antibodies against NKG2D (558071) FC (1:10), 2B4 (562350) FC (1:10), and CD56 (555518) FC (1:10) were procured from BD Biosciences. Mouse antibodies against 2B4 (clone 1.7) NK cell activation (1:40) and CD16 (clone 3G8) NK cell activation (1:20) were purified from ascites.

siRNA constructs and nucleofection

siRNAs used included a control siRNA (siCtrl: 5′-UUCUCCGAA CGUGUCACGU-3′), two siRNAs against septin 2 (1–5′-GAUCCA AUCAGUUGAUUGAAGCCAA-3′ and 2–5′-UGUCCAGAUUGA GGCUUCAACUGUU-3′), and two siRNAs against septin 7 (1–5′-GCUUAUGGUAGUGGGUGAAUCUGGA-3′ and 2–5′-GCUGAG GAGAGGAGCGUCAACAGCA-3′; Thermo Fisher Scientific). Nucleofection of siRNA oligos into NKL and primary human NK cells was done using the standard protocol and Nucleofection V kit (Lonza) and an Amaxa Nucleofector I, as previously described (Phatarpekar et al., 2016). Cells were nucleofected with 600 pmols of siRNA. All subsequent assays were completed 48 (primary human NK cell) or 72 h (NKL) after nucleofection. All knock-down experiments were verified by immunoblotting for decrease in the targeted protein.

CRISPR constructs and nucleofection

CRISPR reagents used comprised of gRNAs, which included a control (5′-GTTCCGCGTTACATAACTTA-3′) and two different gRNAs each against septin 7 (1–5′-CUAUCAAUGUAGUCGAUA ACGUUUUAGAGCUAUGCU-3′ and 2–5′-UGAAUUCACGCUUAU GGUAGGUUUUAGAGCUAUGCU-3′), STX11 (1–5′-UCGAACACG AUGUCCUCGUGGUUUUAGAGCUAUGCU-3′ and 2–5′-GUUCGA GACGGACCACAUCCGUUUUAGAGCUAUGCU-3′), and STXBP2 (1–5′-AGCGGCCUAGCUCACUGAACGUUUUAGAGCUAUGCU-3′ and 2–5′-CCCGACUUUCACCUACAAAGGUUUUAGAGCUAU

GCU-3′); trans-activating crispr RNA (tracrRNA) for Cas9, and Cas9 enzyme (Integrated DNA Technologies). A complex of gRNA and tracrRNA was prepared at a 1:1 ratio by heating at 95°C for 5 min and then cooling to room temperature. For knock-out of each gene, a complex was formed by combining gRNA/tracrRNA complex of each gRNA at a 1:1 ratio with 30 µg of Cas9 enzyme at room temperature for 10 min. NKL cells were nucleofected with the complex using the CM-137 program on a Lonza 4D nucleofector and Nucleofection V kit (Lonza). Cells were nucleofected with 225 pmols of each gRNA. All subsequent assays were completed 96 h after nucleofection. All knock-out experiments were verified by immunoblotting.

Treatment with FCF

NKL and primary NK cells resuspended in NK media were treated with FCF for 3 h at the indicated concentration. For control, cells were treated with an equal volume of DMSO (diluent for FCF).

FC for surface receptor staining

Half a million cells were blocked in 50 µl of 50% FBS in PBS for 15 min at room temperature. After blocking, antibody against the receptor of interest was added, and the cells were stained in the dark for 15 min at room temperature. After staining, cells were washed twice with PBS and fixed with 2% formaldehyde in PBS. Cells were run on a FACSCanto II flow cytometer (BD Biosciences), and the data were analyzed with FlowJo (Tree Star).

Lysosome fractionation

Preparation of the crude lysosome fraction was performed as previously described (Schenkman and Cinti, 1978). NKL cells (200×10^6) were resuspended in 1.5 ml of 0.25 M sucrose in 10 mM Tris (pH 7.4) and homogenized with a dounce tissue homogenizer. The homogenate was spun at 600 *g* for 5 min at 4°C, and the supernatant (post-nuclear lysate) was collected and spun again at 12,000 *g* for 10 min at 4°C. The supernatant was then collected (post-mitochondrial lysate), and $CaCl_2$ was added to the supernatant to a final concentration of 8 mM and mixed well. The mixture was then spun at 14,000 rpm for 15 min at 4°C, and the supernatant was collected as the non-lysosomal fraction ($CaCl_2$). The pellet was washed once with 150 mM KCl in 10 mM Tris (pH 7.4) at 14,000 rpm for 15 min at 4°C, resuspended with 80 µl 150 mM KCl in 10 mM Tris (pH 7.4), and saved as the CLF. Samples from each fraction were separated by SDS-PAGE and immunoblotted as indicated.

Cytotoxicity assay

Chromium (^{51}Cr) release assays were performed as previously described (Ham et al., 2013, 2015). In brief, target 721.221 cells were labeled with ^{51}Cr (Perkin-Elmer) and co-cultured with dilutions of NK cells, and cytotoxicity percent was determined in reference to a standard spontaneous (standard cell culture media) and maximum (0.5% Triton X-100; Sigma-Aldrich) release. All assays were performed for 4 h, and resulting ^{51}Cr release was measured using Luma-96 plates (PerkinElmer), Top-Seal A Plus (PerkinElmer), and Top Count NXT Microplate Scintillation and Luminescence Counter. NK cell reverse antibody-dependent cytotoxicity assays (R-ADCC) were performed using antibodies against NKG2D (R&D Systems), 2B4 (C1.7) and CD16 (3G8), and the P815 cell line, as previously described (Ham et al., 2013).

Conjugate assay

NKL or primary human NK cells treated as indicated (septin depletion or FCF) were labeled with Calcein-AM (Invitrogen) for 1 h with intermittent mixing. Target 721.221 cells were stained with CMAC (Invitrogen) for 30 min in serum-free media with subsequent washing and incubation in complete media. Labeled cells were washed and resuspended in serum-free media at 1.5–3 million cells/ml (NKL and primary human NK cells) and 2.5 million cells/ml (721.221). Cells were incubated on ice for 20 min and then mixed together (250 µl of each) and centrifuged at 200 rpm for 5 min at 4°C without brake and then incubated at 37°C for the indicated amount of time. Conjugate formation was terminated by vigorous vortexing and fixation with 4% paraformaldehyde in PBS. Conjugate formation was assessed using two-color FC on a FACSCanto II flow cytometer (BD Biosciences) and analyzed by quantifying the percentage of target-bound NK cells ($CMAC^+Calcein^+$) from the gated population of total number of NK cells ($Calcein^+$) using Flowjo software (Tree Star).

Degranulation assay

NKL or primary NK cells treated as indicated (septin depletion or FCF) were resuspended in 100 µl serum-free media along with FITC-conjugated andibody against CD107a (BD Biosciences) and 2 µM PMA and 4 µM ionomycin. The cells were incubated at 37°C for 30 min. At the end of incubation, the cells were washed twice with PBS and fixed with 2% formaldehyde in PBS. Degranulation was assessed by FC and analyzed by quantifying the percentage of $CD107a^+$ cells from the gated population of total number of NK cells using FlowJo software (Tree Star).

Cell stimulation

In experiments involving cell surface receptor (NKG2D and 2B4) cross-linking, 10×10^6 NKL cells were prepared for each stimulation condition. 5 µg of anti-NKG2D (R&D Systems) and anti-2B4 (clone C1.7) were added to 100 µl cell suspension and incubated together for 10 min on ice. Washed cells were then incubated with goat anti-mouse IgG $F(ab')_2$ (Cappel) at 37°C for the indicated periods of time. In experiments involving stimulation with PMA and ionomycin, 2 µM of the former and 4 µM of the latter were added to 100 µl cell suspension and incubated for 15 min at 37°C.

IP and immunoblotting

For IP, cells were lysed in lysis buffer (20 mM Hepes, pH 7.2, 50 mM potassium acetate, 1 mM EDTA, 200 mM D-sorbitol and 0.1% Triton X-100, 1 mM sodium orthovanadate, 1 mM PMSF, 10 µg/ml leupeptin, and 5 µg/ml aprotinin). IP was performed using antibody against the protein of interest and protein A Sepharose beads (Sigma-Aldrich) as previously described (Gomez et al., 2005). For immunoblotting, cells were lysed in 10 mM Tris with 50 mM NaCl, 5 mM EDTA, 50 mM sodium fluoride or NAF, 30 mM $Na_4P_2O_7$, and 1% Triton X-100, pH 7.4, and protein concentration was estimated using Bradford assay. Samples were separated by SDS-PAGE and immunoblotted as

indicated. Protein band intensity was quantified using the volume tool in the Image Lab software (Bio-Rad).

Microscopy

NKL or primary NK cells, with or without siRNA nucleofection, were plated onto poly-L-lysine–coated coverslips for 15 min at 37°C. In some instances, treated cells were plated onto fibronectin-coated coverslips, which were made by floating the coverslip over 100 µl of PBS-diluted fibronectin at 1 mg/ml for 2 h at 4°C. Treated coverslips were washed 3× in 1× PBS before use. Conjugates of NKL/primary NK cells and 721.221 were made as described above, with 250 µl of CMAC-stained 721.221 (2.5 million cells/ml; Invitrogen) mixed with 250 µl of NKL/primary human NK cells (1.5–3 million cells/ml) in serum-free media and centrifuged together at 200 rpm without brake for 5 min at 4°C. For single time-point siRNA experiments, cell mixtures were incubated at 37°C for 15 min, resuspended, and allowed to adhere to poly-L-lysine–coated coverslips for an additional 15 min at 37°C. Cells were fixed with molecular grade 4% paraformaldehyde (Electron Microscopy Sciences) in PBS (18 min), permeabilized with 0.15% Surfact-Amps (28314; Thermo Fisher Scientific) in PBS (3 min), blocked with FBS-based blocking reagent, and stained with the indicated antibodies. Secondary reagents included Alexa Fluor 568– and Alexa Fluor 647–conjugated versions of donkey anti-mouse IgG and donkey anti-rabbit IgG antibodies (Invitrogen). F-actin was visualized using Alexa Fluor–conjugated 488 or 647 phalloidin (Invitrogen). Coverslips were mounted onto glass slides using SlowFade (Invitrogen) and examined on a C-Acromat 63×/1.2w or 63×/1.4 oil objective on an LSM-710 or LSM-800 laser scanning confocal microscope with Airyscan (Carl Zeiss). Images were captured using the ZEN blue software package (Carl Zeiss).

Image analysis

Microscopic images were processed and analyzed using ImageJ software (version 1.50i; National Institutes of Health). Fluorescence quantification was done on unadjusted images, in which the cellular structures were difficult to see with the human eye in many cases but would fall in the dynamic range of the software. For all representative images, modifications were consistent within an experiment. The distance of the MTOC to the synapse and the distance of the individual granules to the MTOC were quantified using the ImageJ length function on images adjusted to increase clarity as previously described (Wilton and Billadeau, 2018; Wilton et al., 2019). To quantify the average distance of the granules to the MTOC, the distance of each granule to the MTOC was collected. When granules merged, a series of points representing individual granules in size and location was quantified in a grid pattern. The collective granule distances for each cell were averaged to obtain a single value representing the average granule distance in that cell. These average values were then analyzed as a dataset. Representative images shown are adjusted to increase clarity of the location of the MTOC and granules. For analysis of cell diameter, the line segment tool in ImageJ was used to draw a line along the longest diameter of the cell. The length of the line was obtained using the Analyze–Measure tool. For analysis of septin 7 mean fluorescence intensity (MFI) at the CS, the orthogonal tool was used to outline the synapse, and the MFI was calculated using the Analyze–Measure tool.

PLA

In situ interaction between proteins was assessed by PLA kit Duolink: PLA probe anti-rabbit plus, PLA probe anti-mouse minus (Sigma-Aldrich), following the manufacturer's protocol. In brief, cells plated on the fibronectin-coated coverslips were blocked, permeabilized, and incubated with primary antibodies. For negative controls, only the primary mouse monoclonal antibody was included. Subsequently, cells were incubated with plus and minus probes and later ligated and amplified. Cells were stained with Alexa Fluor 674 phalloidin (Invitrogen) to visualize F-actin. Z-stack images were captured using an LSM-800 laser scanning confocal microscope as indicated above. The images were processed using ImageJ. In some experiments, PLA spots were counted by generating maximum intensity projection of z-stack images, and color channels were split into the F-actin channel and positive reaction spots channel. Based on the F-actin staining, each cell was outlined and added to the region of interest manager. Using default threshold values, positive reaction spots in the outlined cell were counted using the analyze particle tool. Data distribution was assumed to be normal but not formally tested.

Statistical analysis

All statistical analyses in this study were performed using the two-tailed Student's *t* test, or one-way ANOVA with Dunnett's multiple comparison in GraphPad Prism. Data distribution was assumed to be normal but was not formally tested.

Online supplemental material

Fig. S1 extends the characterization of the localization of septin 7 at the NKL–721.221 contact site and anti-septin 7 antibody validation in Fig. 1. The impact of FCF treatment and depletion of septin 2 on NK cell cytotoxicity are presented in Fig. S2 and extend Fig. 3. The impact of FCF treatment on activating receptor expression and signaling are shown in Fig. S3 and extend Fig. 4. Fig. S4 shows the impact of septin 7 depletion on other septin proteins and extends data shown in Fig. 3. Fig. S5 demonstrates the impact of FCF treatment on fibronectin-induced spreading and conjugate formation extend data shown in Fig. 4. Video 1 shows a 3D reconstruction of an NK–721.221 conjugate showing diminished septin 7 IF at the CS and extends Fig. 2 B. Video 2 shows a 3D reconstruction of septin 7 and STX11 PLA assay in NKL–721.221 conjugate and extends Fig. 7 D.

Acknowledgments

This work was supported by the Mayo Foundation for Medical Education and Research and National Institute of Allergy and Infectious Diseases grant R01-AI120949 (to D.D. Billadeau). We also acknowledge support from the Proteomics Shared Resources of the Mayo Clinic Cancer Center grant P30 CA015083.

The authors declare no competing financial interests.

Author contributions: Conceptualization: P.V. Phatarpekar and D.D. Billadeau; Methodology: P.V. Phatarpekar, B.L. Overlee, and D.D. Billadeau; Investigation: P.V. Phatarpekar, B.L. Overlee, K.M. Wilton, H. Ham, A. Leehan, and D.D. Billadeau; Formal Analysis: P.V. Phatarpekar, B.L. Overlee, and D.D. Billadeau; Resources: P.V. Phatarpekar, B.L. Overlee, and D.D. Billadeau; Writing – Original Draft: P.V. Phatarpekar and D.D. Billadeau; Writing – Review and Editing: D.D. Billadeau; Visualization: P.V. Phatarpekar and D.D. Billadeau; Supervision: D.D. Billadeau; Funding Acquisition: D.D. Billadeau.

Submitted: 25 February 2020
Revised: 26 June 2020
Accepted: 28 July 2020

References

Arneson, L.N., A. Brickshawana, C.M. Segovis, R.A. Schoon, C.J. Dick, and P.J. Leibson. 2007. Cutting edge: syntaxin 11 regulates lymphocyte-mediated secretion and cytotoxicity. *J. Immunol.* 179:3397–3401. https://doi.org/10.4049/jimmunol.179.6.3397

Beber, A., C. Taveneau, M. Nania, F.C. Tsai, A. Di Cicco, P. Bassereau, D. Lévy, J.T. Cabral, H. Isambert, S. Mangenot, et al. 2019. Membrane reshaping by micrometric curvature sensitive septin filaments. *Nat. Commun.* 10: 420. https://doi.org/10.1038/s41467-019-08344-5

Beise, N., and W. Trimble. 2011. Septins at a glance. *J. Cell Sci.* 124:4141–4146. https://doi.org/10.1242/jcs.087007

Beites, C.L., H. Xie, R. Bowser, and W.S. Trimble. 1999. The septin CDCrel-1 binds syntaxin and inhibits exocytosis. *Nat. Neurosci.* 2:434–439. https://doi.org/10.1038/8100

Beites, C.L., K.A. Campbell, and W.S. Trimble. 2005. The septin Sept5/CDCrel-1 competes with alpha-SNAP for binding to the SNARE complex. *Biochem. J.* 385:347–353. https://doi.org/10.1042/BJ20041090

Biggs, C.M., S. Keles, and T.A. Chatila. 2017. DOCK8 deficiency: Insights into pathophysiology, clinical features and management. *Clin. Immunol.* 181: 75–82. https://doi.org/10.1016/j.clim.2017.06.003

Billadeau, D.D., K.M. Brumbaugh, C.J. Dick, R.A. Schoon, X.R. Bustelo, and P.J. Leibson. 1998. The Vav-Rac1 pathway in cytotoxic lymphocytes regulates the generation of cell-mediated killing. *J. Exp. Med.* 188:549–559. https://doi.org/10.1084/jem.188.3.549

Bridges, A.A., and A.S. Gladfelter. 2015. Septin Form and Function at the Cell Cortex. *J. Biol. Chem.* 290:17173–17180. https://doi.org/10.1074/jbc.R114.634444

Bryceson, Y.T., E. Rudd, C. Zheng, J. Edner, D. Ma, S.M. Wood, A.G. Bechensteen, J.J. Boelens, T. Celkan, R.A. Farah, et al. 2007. Defective cytotoxic lymphocyte degranulation in syntaxin-11 deficient familial hemophagocytic lymphohistiocytosis 4 (FHL4) patients. *Blood.* 110: 1906–1915. https://doi.org/10.1182/blood-2007-02-074468

Degroote, R.L., S.M. Hauck, B. Amann, S. Hirmer, M. Ueffing, and C.A. Deeg. 2014. Unraveling the equine lymphocyte proteome: differential septin 7 expression associates with immune cells in equine recurrent uveitis. *PLoS One.* 9. e91684. https://doi.org/10.1371/journal.pone.0091684

Dressel, R., L. Elsner, P. Novota, N. Kanwar, and G. Fischer von Mollard. 2010. The exocytosis of lytic granules is impaired in Vti1b- or Vamp8-deficient CTL leading to a reduced cytotoxic activity following antigen-specific activation. *J. Immunol.* 185:1005–1014. https://doi.org/10.4049/jimmunol.1000770

Elstak, E.D., M. Neeft, N.T. Nehme, J. Voortman, M. Cheung, M. Goodarzifard, H.C. Gerritsen, P.M. van Bergen En Henegouwen, I. Callebaut, G. de Saint Basile, et al. 2011. The munc13-4-rab27 complex is specifically required for tethering secretory lysosomes at the plasma membrane. *Blood.* 118:1570–1578. https://doi.org/10.1182/blood-2011-02-339523

Farrugia, A.J., and F. Calvo. 2017. Cdc42 regulates Cdc42EP3 function in cancer-associated fibroblasts. *Small GTPases.* 8:49–57. https://doi.org/10.1080/21541248.2016.1194952

Feldmann, J., I. Callebaut, G. Raposo, S. Certain, D. Bacq, C. Dumont, N. Lambert, M. Ouachée-Chardin, G. Chedeville, H. Tamary, et al. 2003. Munc13-4 is essential for cytolytic granules fusion and is mutated in a form of familial hemophagocytic lymphohistiocytosis (FHL3). *Cell.* 115: 461–473. https://doi.org/10.1016/S0092-8674(03)00855-9

Gilden, J., and M.F. Krummel. 2010. Control of cortical rigidity by the cytoskeleton: emerging roles for septins. *Cytoskeleton (Hoboken).* 67:477–486.

Gilden, J.K., S. Peck, Y.C. Chen, and M.F. Krummel. 2012. The septin cytoskeleton facilitates membrane retraction during motility and blebbing. *J. Cell Biol.* 196:103–114. https://doi.org/10.1083/jcb.201105127

Gomez, T.S., M.J. Hamann, S. McCarney, D.N. Savoy, C.M. Lubking, M.P. Heldebrant, C.M. Labno, D.J. McKean, M.A. McNiven, J.K. Burkhardt, et al. 2005. Dynamin 2 regulates T cell activation by controlling actin polymerization at the immunological synapse. *Nat. Immunol.* 6:261–270. https://doi.org/10.1038/ni1168

Ham, H., S. Guerrier, J. Kim, R.A. Schoon, E.L. Anderson, M.J. Hamann, Z. Lou, and D.D. Billadeau. 2013. Dedicator of cytokinesis 8 interacts with talin and Wiskott-Aldrich syndrome protein to regulate NK cell cytotoxicity. *J. Immunol.* 190:3661–3669. https://doi.org/10.4049/jimmunol.1202792

Ham, H., W. Huynh, R.A. Schoon, R.D. Vale, and D.D. Billadeau. 2015. HkRP3 is a microtubule-binding protein regulating lytic granule clustering and NK cell killing. *J. Immunol.* 194:3984–3996. https://doi.org/10.4049/jimmunol.1402897

Hellewell, A.L., O. Foresti, N. Gover, M.Y. Porter, and E.W. Hewitt. 2014. Analysis of familial hemophagocytic lymphohistiocytosis type 4 (FHL-4) mutant proteins reveals that S-acylation is required for the function of syntaxin 11 in natural killer cells. *PLoS One.* 9. e98900. https://doi.org/10.1371/journal.pone.0098900

Hsu, S.C., C.D. Hazuka, R. Roth, D.L. Foletti, J. Heuser, and R.H. Scheller. 1998. Subunit composition, protein interactions, and structures of the mammalian brain sec6/8 complex and septin filaments. *Neuron.* 20: 1111–1122. https://doi.org/10.1016/S0896-6273(00)80493-6

Hu, Q., W.J. Nelson, and E.T. Spiliotis. 2008. Forchlorfenuron alters mammalian septin assembly, organization, and dynamics. *J. Biol. Chem.* 283: 29563–29571. https://doi.org/10.1074/jbc.M804962200

Huang, Y.W., M. Yan, R.F. Collins, J.E. Diciccio, S. Grinstein, and W.S. Trimble. 2008. Mammalian septins are required for phagosome formation. *Mol. Biol. Cell.* 19:1717–1726. https://doi.org/10.1091/mbc.e07-07-0641

Joberty, G., R.R. Perlungher, P.J. Sheffield, M. Kinoshita, M. Noda, T. Haystead, and I.G. Macara. 2001. Borg proteins control septin organization and are negatively regulated by Cdc42. *Nat. Cell Biol.* 3:861–866. https://doi.org/10.1038/ncb1001-861

Kinoshita, A., M. Noda, and M. Kinoshita. 2000. Differential localization of septins in the mouse brain. *J. Comp. Neurol.* 428:223–239. https://doi.org/10.1002/1096-9861(20001211)428:2<223::AID-CNE3>3.0.CO;2-M

Lassen, L.B., A. Füchtbauer, A. Schmitz, A.B. Sørensen, F.S. Pedersen, and E.M. Füchtbauer. 2013. Septin9 is involved in T-cell development and CD8+ T-cell homeostasis. *Cell Tissue Res.* 352:695–705. https://doi.org/10.1007/s00441-013-1618-6

Mentlik, A.N., K.B. Sanborn, E.L. Holzbaur, and J.S. Orange. 2010. Rapid lytic granule convergence to the MTOC in natural killer cells is dependent on dynein but not cytolytic commitment. *Mol. Biol. Cell.* 21:2241–2256. https://doi.org/10.1091/mbc.e09-11-0930

Mostowy, S., and P. Cossart. 2012. Septins: the fourth component of the cytoskeleton. *Nat. Rev. Mol. Cell Biol.* 13:183–194. https://doi.org/10.1038/nrm3284

Mujal, A.M., J.K. Gilden, A. Gérard, M. Kinoshita, and M.F. Krummel. 2016. A septin requirement differentiates autonomous and contact-facilitated T cell proliferation. *Nat. Immunol.* 17:315–322. https://doi.org/10.1038/ni.3330

Nurullin, L.F., V.F. Khuzakhmetova, E.F. Khaziev, D.V. Samigullin, A.N. Tsentsevitsky, A.I. Skorinkin, E.A. Bukharaeva, and O. Vagin. 2019. Reorganization of Septins Modulates Synaptic Transmission at Neuromuscular Junctions. *Neuroscience.* 404:91–101. https://doi.org/10.1016/j.neuroscience.2019.01.060

O'Loughlin, T., T.A. Masters, and F. Buss. 2018. The MYO6 interactome reveals adaptor complexes coordinating early endosome and cytoskeletal dynamics. *EMBO Rep.* 19. e44884. https://doi.org/10.15252/embr.201744884

Orange, J.S.. 2008. Formation and function of the lytic NK-cell immunological synapse. *Nat. Rev. Immunol.* 8:713–725. https://doi.org/10.1038/nri2381

Orange, J.S., K.E. Harris, M.M. Andzelm, M.M. Valter, R.S. Geha, and J.L. Strominger. 2003. The mature activating natural killer cell immunologic synapse is formed in distinct stages. *Proc. Natl. Acad. Sci. USA.* 100: 14151–14156. https://doi.org/10.1073/pnas.1835830100

Peng, X.R., Z. Jia, Y. Zhang, J. Ware, and W.S. Trimble. 2002. The septin CDCrel-1 is dispensable for normal development and neurotransmitter release. *Mol. Cell. Biol.* 22:378–387. https://doi.org/10.1128/MCB.22.1.378-387.2002

Pettmann, J., A.M. Santos, O. Dushek, and S.J. Davis. 2018. Membrane Ultrastructure and T Cell Activation. *Front. Immunol.* 9:2152. https://doi.org/10.3389/fimmu.2018.02152

Phatarpekar, P.V., D.A. Lee, and S.S. Somanchi. 2016. Electroporation of siRNA to Silence Gene Expression in Primary NK Cells. *Methods Mol. Biol.* 1441:267–276. https://doi.org/10.1007/978-1-4939-3684-7_22

Ribet, D., S. Boscaini, C. Cauvin, M. Siguier, S. Mostowy, A. Echard, and P. Cossart. 2017. SUMOylation of human septins is critical for septin filament bundling and cytokinesis. *J. Cell Biol.* 216:4041–4052. https://doi.org/10.1083/jcb.201703096

Rittmeyer, E.N., S. Daniel, S.C. Hsu, and M.A. Osman. 2008. A dual role for IQGAP1 in regulating exocytosis. *J. Cell Sci.* 121:391–403. https://doi.org/10.1242/jcs.016881

Schauer, M., K.J.H. Kleinwort, R.L. Degroote, C. Wiedemann, E. Kremmer, S.M. Hauck, and C.A. Deeg. 2018. Interaction of septin 7 and DOCK8 in equine lymphocytes reveals novel insights into signaling pathways associated with autoimmunity. *Sci. Rep.* 8:12332. https://doi.org/10.1038/s41598-018-30753-7

Schenkman, J.B., and D.L. Cinti. 1978. Preparation of microsomes with calcium. *Methods Enzymol.* 52:83–89. https://doi.org/10.1016/S0076-6879(78)52008-9

Segovis, C.M., R.A. Schoon, C.J. Dick, L.P. Nacusi, P.J. Leibson, and D.D. Billadeau. 2009. PI3K links NKG2D signaling to a CrkL pathway involved in natural killer cell adhesion, polarity, and granule secretion. *J. Immunol.* 182:6933–6942. https://doi.org/10.4049/jimmunol.0803840

Sellin, M.E., P. Holmfeldt, S. Stenmark, and M. Gullberg. 2011. Microtubules support a disk-like septin arrangement at the plasma membrane of mammalian cells. *Mol. Biol. Cell.* 22:4588–4601. https://doi.org/10.1091/mbc.e11-09-0754

Sheffield, P.J., C.J. Oliver, B.E. Kremer, S. Sheng, Z. Shao, and I.G. Macara. 2003. Borg/septin interactions and the assembly of mammalian septin heterodimers, trimers, and filaments. *J. Biol. Chem.* 278:3483–3488. https://doi.org/10.1074/jbc.M209701200

Spessott, W.A., M.L. Sanmillan, M.E. McCormick, N. Patel, J. Villanueva, K. Zhang, K.E. Nichols, and C.G. Giraudo. 2015. Hemophagocytic lymphohistiocytosis caused by dominant-negative mutations in STXBP2 that inhibit SNARE-mediated membrane fusion. *Blood.* 125:1566–1577. https://doi.org/10.1182/blood-2014-11-610816

Spessott, W.A., M.L. Sanmillan, M.E. McCormick, V.V. Kulkarni, and C.G. Giraudo. 2017. SM protein Munc18-2 facilitates transition of Syntaxin 11-mediated lipid mixing to complete fusion for T-lymphocyte cytotoxicity. *Proc. Natl. Acad. Sci. USA.* 114:E2176–E2185. https://doi.org/10.1073/pnas.1617981114

Spiliotis, E.T.. 2018. Spatial effects - site-specific regulation of actin and microtubule organization by septin GTPases. *J. Cell Sci.* 131. jcs207555. https://doi.org/10.1242/jcs.207555

Tang, B.L.. 2015. A unique SNARE machinery for exocytosis of cytotoxic granules and platelets granules. *Mol. Membr. Biol.* 32:120–126. https://doi.org/10.3109/09687688.2015.1079934

Tokhtaeva, E., J. Capri, E.A. Marcus, J.P. Whitelegge, V. Khuzakhmetova, E. Bukharaeva, N. Deiss-Yehiely, L.A. Dada, G. Sachs, E. Fernandez-Salas, et al. 2015. Septin dynamics are essential for exocytosis. *J. Biol. Chem.* 290:5280–5297. https://doi.org/10.1074/jbc.M114.616201

Tooley, A.J., J. Gilden, J. Jacobelli, P. Beemiller, W.S. Trimble, M. Kinoshita, and M.F. Krummel. 2009. Amoeboid T lymphocytes require the septin cytoskeleton for cortical integrity and persistent motility. *Nat. Cell Biol.* 11:17–26. https://doi.org/10.1038/ncb1808

Vivier, E., E. Tomasello, M. Baratin, T. Walzer, and S. Ugolini. 2008. Functions of natural killer cells. *Nat. Immunol.* 9:503–510. https://doi.org/10.1038/ni1582

Wilton, K.M., and D.D. Billadeau. 2018. VASP Regulates NK Cell Lytic Granule Convergence. *J. Immunol.* 201:2899–2909. https://doi.org/10.4049/jimmunol.1800254

Wilton, K.M., B.L. Overlee, and D.D. Billadeau. 2019. NKG2D-DAP10 signaling recruits EVL to the cytotoxic synapse to generate F-actin and promote NK cell cytotoxicity. *J. Cell Sci.* 133. jcs230508.

Yadav, S., J.A. Oses-Prieto, C.J. Peters, J. Zhou, S.J. Pleasure, A.L. Burlingame, L.Y. Jan, and Y.N. Jan. 2017. TAOK2 Kinase Mediates PSD95 Stability and Dendritic Spine Maturation through Septin7 Phosphorylation. *Neuron.* 93:379–393. https://doi.org/10.1016/j.neuron.2016.12.006

Supplemental material

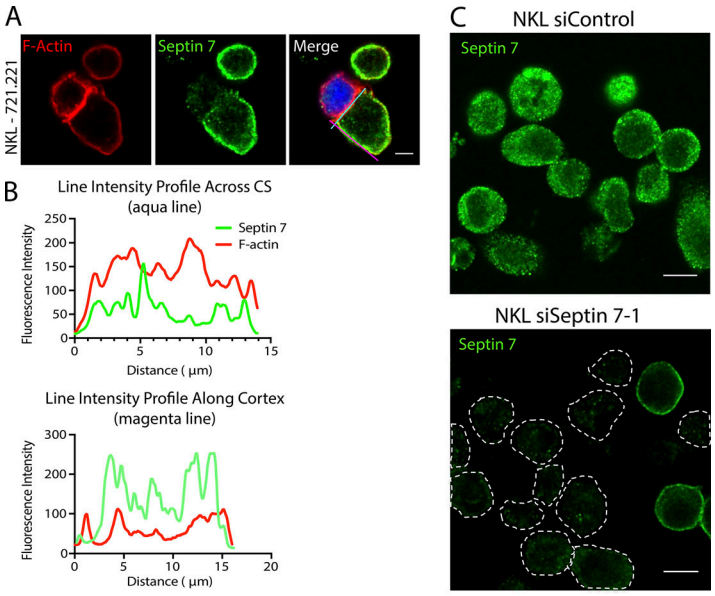

Figure S1. **Septin 7 primarily accumulates within the cell cortex away from the CS. (A)** NKL cells were allowed to form conjugates with CMAC-labeled 721.221 cells (blue) and stained for F-actin (red) or septin 7 (green) and imaged using confocal microscopy. Scale bar, 5 µm. **(B)** Line intensities profiles were created from the aqua line at the CS and magenta line along the NK cell cortex in images from A using Fiji. **(C)** Primary human NK cells were nucleofected with either control or septin 7–1 siRNA. 72 h after nucleofection, cells were placed on to poly-L-lysine–coated coverslips, fixed, stained with anti–septin 7, and imaged by confocal microscopy. Dotted lines in the bottom panel denote the outline of the NK cell. Scale bar, 10 µm.

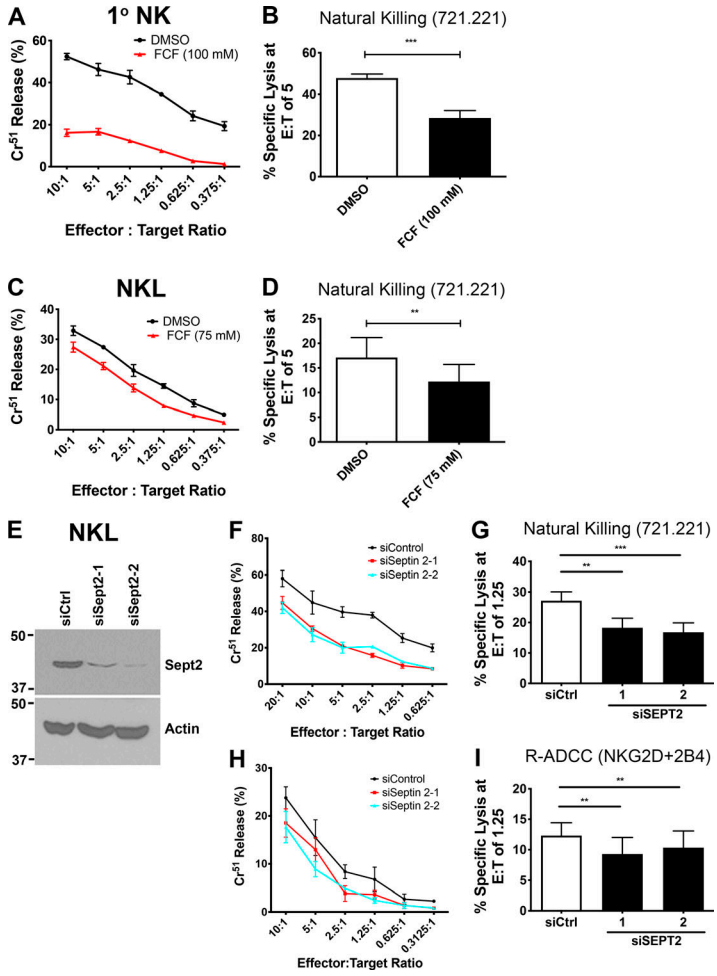

Figure S2. **Septin filament dynamics and septin filament formation are required for NK cell cytotoxicity. (A and C)** DMSO- (control) or FCF-treated cells were incubated at 37°C for 3 h with ^{51}Cr-labeled 721.221 cells at the indicated E:T ratios, and specific lysis was calculated. **(B and D)** Results were quantified for an E:T ratio of five effectors to one target cell over six independent experiments. **(E–I)** NKL cells were nucleofected with siCtrl or siRNAs targeting septin 2. Immunoblot is cropped for clarity. **(E)** 72 h after nucleofection, levels of septin 2 protein were assessed by immunoblot for each experiment. **(F)** Cytolytic activity of nucleofected cells against ^{51}Cr-labeled 721.221 cells was measured as indicated above. **(G)** Results were quantified for an E:T ratio of 1.25 effectors to one target cell over four independent experiments. **(H)** Nucleofected NKL cells were incubated with ^{51}Cr-labeled p815 cells coated with anti-NKG2D + anti-2B4. Percent specific lysis was calculated. **(I)** Results were quantified at an E:T ratio of 1.25 over four independent experiments. All experiments were completed in triplicate or quadruplicate and in reference to spontaneous and total lysis. Results show representative experiments (A, C, E, F, and H) or average values over multiple experiments (B, D, G, and I). Error bars indicate SEM. **, P < 0.005; ***, P < 0.0005 compared with control group. P values indicated are for paired, two-tailed Student's *t* test.

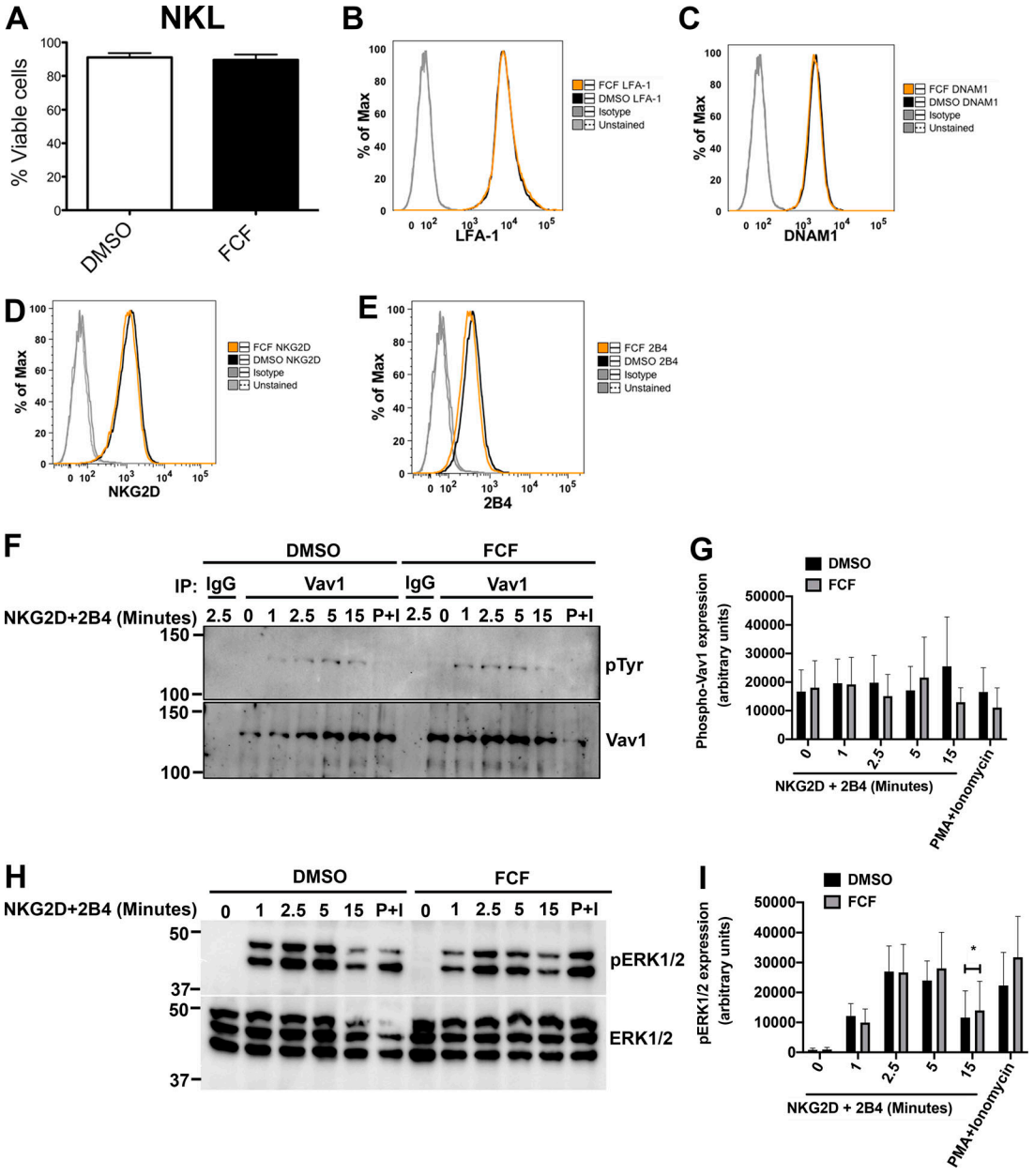

Figure S3. **Stabilization of septin filaments does not affect cell viability, surface expression of activating receptors, and signaling.** NKL cells were treated with DMSO or 75 µM FCF for 3 h. **(A)** Cell viability was assessed. Results shown are the average of three independent experiments. Error bars indicate SEM. **(B–E)** Surface expression of activating receptors was measured using FC. Flow charts shown are representative of two independent experiments, each performed in triplicate. **(F–I)** NKL Cells were stimulated over the indicated time course by ligation of NKG2D/2B4 receptors or with PMA (2 µM) and ionomycin (4 µM; P+I) for 15 min. **(F)** Cell lysates were immunoprecipitated (IP) with anti-Vav1 or rabbit IgG, and activated Vav1 was detected by immunoblotting with anti-phosphotyrosine (pTyr) antibody. **(G)** Phospho-Vav1 bands were quantified using Bio-Rad Image Lab software and normalized to Vav1 expression. **(H)** Activated cells were immunoblotted as indicated. **(I)** Phospho-ERK1/2 (pERK1/2) bands were quantified and normalized to ERK1/2 expression. Blots shown are representative of three independent experiments. Error bars indicate SEM. *, $P < 0.05$. P values indicated are for paired, two-tailed Student's *t* test.

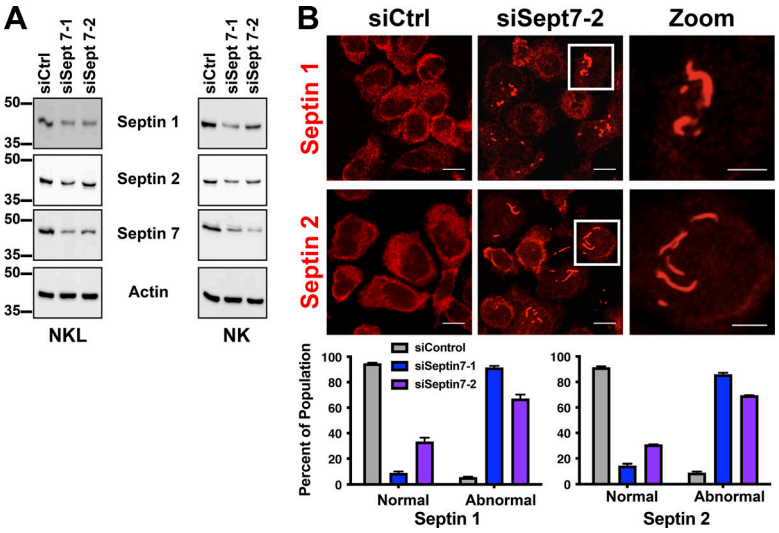

Figure S4. **Depletion of septin 7 results in the formation of abnormal septin filaments. (A)** Primary NK cells or NKL were nucleofected with the indicated siRNAs. 72 h after nucleofection, cells were lysed, clarified, and then subjected to SDS-PAGE followed by immunoblotting for the indicated proteins. **(B)** Primary NK cells nucleofected with the indicated siRNAs were plated onto fibronectin-coated coverslips 72 h after nucleofection. Cells were fixed and stained with antibodies against septin 1 and septin 2 and imaged using confocal microscopy. Representative images are shown. Scale bar, 10 µm; inset scale bar, 5 µm. Primary NK cells imaged in B were quantified for containing either normal septin 1 or septin 2 structures or abnormal septin structures. 50 cells were quantified for each condition over three independent experiments.

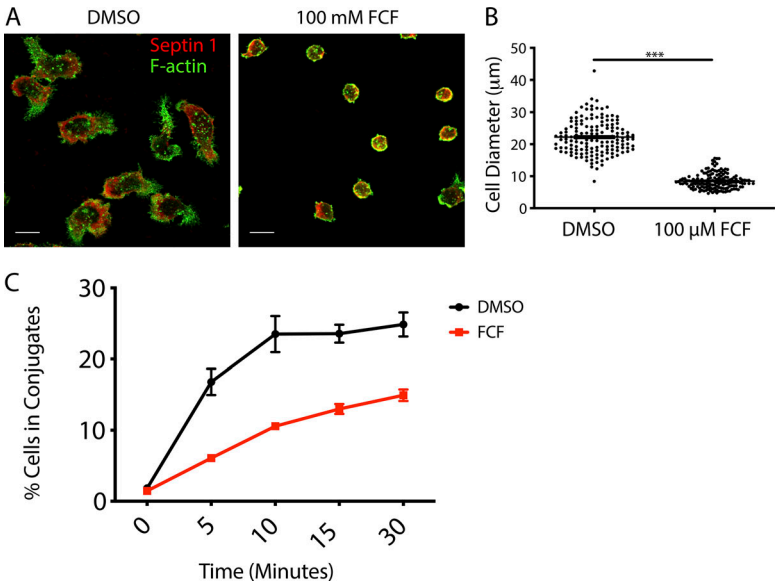

Figure S5. **FCF blocks impairs fibronectin-induced cell spreading and abrogates conjugate formation. (A)** Primary NK cells were treated with diluent (DMSO) or 100 mM FCF for 2 h and then dropped onto fibronectin-coated coverslips and allowed to adhere and spread for 15 min at 37°C in a humidified chamber. The coverslips were subsequently fixed and stained with anti–septin 1 (red) and phalloidin to detect F-actin (green). Representative images from three independent experiments are shown. Scale bar, 10 µm. **(B)** The diameter of the cell along its longest access was measured using ImageJ. Data represent three independent experiments in which the diameter of 50 cells was calculated. ***, $P < 0.05$ as determined using the unpaired two-tailed Student's *t* test. **(C)** NKL cells were stained with Calcein-AM and then allowed to form conjugates at 37°C with CMAC-labeled 721.221 cells over the specified times and then fixed. The formation of conjugates (CMAC + Calcein-AM$^+$) with respect to the total number of NKL cells (Calcein-AM$^+$) was assessed using two-color FC. Results shown are the representative of three independent experiments, each performed in triplicate.

Video 1. **3D reconstruction of an NK-721.221 conjugate showing diminished septin 7 IF at the CS.** Septin 7, green; F-actin, red; 721.221, blue.

Video 2. **3D reconstruction of septin 7 and STX11 PLA assay in NKL–721.221 conjugate.** PLA, red; F-actin, cyan; 721.211, gray.